

1 **Short title:** Simultaneous ER and cytosol Ca<sup>2+</sup> imaging

2

3 **Corresponding author** Alex Costa, alex.costa@unimi.it

4 Department of Biosciences

5 University of Milan

6 Via Celoria 26, I-20133, Milan, Italy

7 Tel. +39 2503 14831

8

9 **Simultaneous imaging of ER and cytosolic Ca<sup>2+</sup> dynamics reveals long-**  
10 **distance ER Ca<sup>2+</sup> waves in plants**

11

12 **Francesca Resentini<sup>1,§</sup>, Matteo Grenzi<sup>1,§</sup>, Daniele Ancora<sup>2</sup>, Mara Cademartori<sup>1</sup>, Laura Luoni<sup>1</sup>,**  
13 **Marianna Franco<sup>1</sup>, Andrea Bassi<sup>2</sup>, Maria Cristina Bonza<sup>1</sup>, Alex Costa<sup>1,3,\*</sup>**

14 <sup>1</sup>Department of Biosciences, University of Milan, Via G. Celoria 26, 20133 Milan, Italy

15 <sup>2</sup>Department of Physics, Politecnico di Milano, 20133 Milano, Italy

16 <sup>3</sup>Institute of Biophysics, Consiglio Nazionale delle Ricerche, Via G. Celoria 26, 20133 Milan, Italy

17

18 <sup>§</sup>These authors contributed equally to this work

19 \*Corresponding author: [alex.costa@unimi.it](mailto:alex.costa@unimi.it)

20

21 **One-sentence summary:** Dual color imaging allows the simultaneous analysis of calcium dynamics  
22 in the endoplasmic reticulum and cytosol from single cells to adult entire plants.

23

24 **FOOTNOTES**

25

26 **Author Contributions**

27 AC and MCB conceived the project with specific input from FR, MG, and AB. MG and AC designed  
28 the experiments. FR, MC, and MF generated the constructs. FR, MG, and MF performed and  
29 analyzed the experiments. FR and LL generated the transgenic lines. DA and AB performed cross-  
30 correlation analyses of Fig. 2 and temporal evolution of signals in Fig. 4. AC and MG prepared the  
31 Figures and Videos. AC and MCB wrote the manuscript with input from all co-authors. AC agrees to  
32 serve as the author responsible for contact and ensures communication.

33

34 **Funding Information**

35 This work was supported by Piano di Sviluppo di Ateneo 2019 (University of Milan) (to AC), by  
36 Ministero dell'Istruzione, dell'Università e della Ricerca Fondo per Progetti di ricerca di Rilevante  
37 Interesse Nazionale 2017 (PRIN 2017ZBBYNC) (to MCB), and by a PhD fellowship from the  
38 University of Milan (to MG). We acknowledge fundings from H2020 Marie Skłodowska-Curie Actions  
39 (HI-PHRET project, 799230) (to DA).

40

41 **ORCID identifiers:**

42 FR 0000-0003-0033-6930; MG 0000-0003-2295-0018; LL, 0000-0002-6485-5417; AB, 0000-0002-  
43 5017-0775; MCB, 0000-0001-7096-2967; AC, 0000-0002-2628-1176.

44

45 **ABSTRACT**

46 Calcium ions ( $\text{Ca}^{2+}$ ) play a key role in cell signaling across organisms. In plants, a plethora of  
47 environmental and developmental stimuli induce specific  $\text{Ca}^{2+}$  increases in the cytosol as well as in  
48 different cellular compartments including the endoplasmic reticulum (ER). The ER represents an  
49 intracellular  $\text{Ca}^{2+}$  store that actively accumulates  $\text{Ca}^{2+}$  taken up from the cytosol. By exploiting state-of-  
50 the-art genetically encoded  $\text{Ca}^{2+}$  indicators (GECIs), specifically the ER-GCaMP6-210 and R-GECO1,  
51 we report the generation and characterization of an *Arabidopsis* (*Arabidopsis thaliana*) line that allows  
52 for simultaneous imaging of  $\text{Ca}^{2+}$  dynamics in both the ER and cytosol at different spatial scales. By  
53 performing analyses in single cells, we precisely quantified i) the time required by the ER to import  
54  $\text{Ca}^{2+}$  from the cytosol into the lumen; and ii) the time required to observe a cytosolic  $\text{Ca}^{2+}$  increase  
55 upon the pharmacological inhibition of the ER-localized type IIA  $\text{Ca}^{2+}$ -ATPases. Furthermore, live  
56 imaging of mature, soil-grown plants revealed the existence of a wounding-induced, long-distance ER  
57  $\text{Ca}^{2+}$  wave propagating in injured and systemic rosette leaves. This technology enhances high-  
58 resolution analyses of intracellular  $\text{Ca}^{2+}$  dynamics at the cellular level and in adult organisms and  
59 paves the way to develop new methodologies aimed at defining the contribution of subcellular  
60 compartments in  $\text{Ca}^{2+}$  homeostasis and signaling.

## 61 INTRODUCTION

62 In animals, besides its role in protein secretion, the endoplasmic reticulum (ER) is a calcium ( $\text{Ca}^{2+}$ )  
63 store participating in the generation and shaping of stimulus-induced cytosolic  $\text{Ca}^{2+}$  increases  
64 (Soboloff et al., 2012). Moreover, in animals, Ryanodine (RyR) and Inositol trisphosphate ( $\text{InsP}_3\text{R}$ )  
65 receptors are ER-localized, ligand-gated  $\text{Ca}^{2+}$  permeable channels that release  $\text{Ca}^{2+}$  into the cytosol  
66 (Foskett et al., 2007), whereas the ER  $\text{Ca}^{2+}$  refilling is dependent on the activity of sarco/endoplasmic  
67 reticulum  $\text{Ca}^{2+}$ -ATPases (SERCA) and the Stromal Interaction Molecule (STIM)-Orai protein complex  
68 (Soboloff et al., 2012). In plants, RyR,  $\text{InsP}_3\text{R}$ , and the STIM-Orai complex are not present (Edel et al.,  
69 2017). However, a battery of P-Type IIA (ER-type  $\text{Ca}^{2+}$ -ATPases, ECAs) and IIB (Autoinhibited  $\text{Ca}^{2+}$   
70 ATPases, ACAs)  $\text{Ca}^{2+}$ -ATPases are localized in the ER membranes and their primary function is to  
71 import  $\text{Ca}^{2+}$  into the ER lumen (Bonza and De Michelis, 2011, Bonza et al., 2013; Shkolnik et al.,  
72 2018). In addition,  $\text{Ca}^{2+}$ -permeable channels (e.g. Cyclic Nucleotide Gated Channels, CNGC)  
73 localized in the nuclear envelope (NE, which is in continuity with the ER) (Charpentier et al., 2016;  
74 Leitao et al., 2019) and  $\text{Ca}^{2+}$ /Cation transporters (e.g. CCXs) have been shown to participate in the  
75 regulation of  $\text{Ca}^{2+}$  transport across the ER membranes (Corso et al., 2018).

76  $\text{Ca}^{2+}$  transport over the ER membrane was observed using purified microsomal vesicles loaded with  
77 the  $^{45}\text{Ca}^{2+}$  isotope (Navazio et al., 2000). Later, by using Förster resonance energy transfer (FRET)-  
78 based genetically encoded  $\text{Ca}^{2+}$  indicator (GECI) (SP-YC4.6 and CRT-D4ER Cameleon) localized to  
79 the ER lumen, the ER resting  $\text{Ca}^{2+}$  concentration ( $[\text{Ca}^{2+}]$ ) was measured *in vivo* in Arabidopsis  
80 (*Arabidopsis thaliana*) pollen tubes and in leaf and root cells (Iwano et al., 2009; Bonza et al., 2013;  
81 Tian et al., 2014). By using the ratiometric CRT-D4ER Cameleon, we previously reported, in root-tip  
82 cells, the ER  $\text{Ca}^{2+}$  dynamics in response to different stimuli, such as external adenosine triphosphate  
83 (ATP), L-Glutamate, salt stress, and water potential gradient (Bonza et al., 2013, Corso et al., 2018;  
84 Shkolnik et al., 2018). Some of these data were later confirmed by Luo and colleagues (2020), who  
85 generated a new Arabidopsis line expressing the intensiometric ER-localized sensor R-CEPIA1er (Luo  
86 et al., 2020).

87 Overall, in plants, *in vivo* analyses of ER  $\text{Ca}^{2+}$  dynamics revealed that it primarily acts as a  $\text{Ca}^{2+}$  sink,  
88 thus contributing to the dampening of the  $\text{Ca}^{2+}$  transient (Bonza et al., 2013; Corso et al., 2018).  
89 However, ER can also work as a  $\text{Ca}^{2+}$  source, being responsible for the generation of a cytosolic  $\text{Ca}^{2+}$   
90 transient (Shkolnik et al., 2018; Luo et al., 2020).

91 Here we report the successful use of spectral variants of the new generation of intensimetric single  
92 fluorescent protein GECIs (e.g. ER-GCaMP6-210 and R-GECO1) to perform simultaneous imaging of  
93  $\text{Ca}^{2+}$  dynamics in the ER and cytosol. We demonstrate this method in single plant cells as well as in  
94 adult plants.

95

## 96 **RESULTS AND DISCUSSION**

97 Over the years, we have exploited the use of the ratiometric FRET-based CRT-D4ER Cameleon to  
98 study  $\text{Ca}^{2+}$  dynamics in the ER lumen of wild-type and mutant Arabidopsis plants (Bonza et al., 2013;  
99 Corso et al., 2018; Shkolnik et al., 2018). This ratiometric sensor proved to be highly reliable to  
100 highlight different ER  $[\text{Ca}^{2+}]$  at resting and in reporting ER  $\text{Ca}^{2+}$  dynamics in response to various  
101 stimuli in different mutants (Corso et al., 2018; Shkolnik et al., 2018). However, in Arabidopsis, the use  
102 of the CRT-D4ER sensor showed some limitations. Firstly, for reasons not yet investigated, the CRT-  
103 D4ER sensor showed a varying degree of silencing. Despite the use of different promoters and vector  
104 backbones, we failed to detect the expression of the sensor in adult Arabidopsis plants (A. Costa. and  
105 L. Luoni, unpublished data). Only when we expressed the sensor in the *rdr6-11* Arabidopsis  
106 background, which is impaired in gene silencing (Peragine et al., 2004), we detected the sensor  
107 expression in leaves of adult plants (A. Costa and L. Luoni, unpublished data). Due to these  
108 limitations, we could only study the ER  $\text{Ca}^{2+}$  dynamics in young seedlings (Bonza et al., 2013; Corso  
109 et al., 2018; Shkolnik et al., 2018). Secondly, in some cases, we were unable to obtain knockout  
110 mutants expressing the sensor (Corso et al., 2018).

111 In order to choose a highly sensitive sensor to perform the analysis of ER  $\text{Ca}^{2+}$  in different cell types,  
112 which is also usable in a simple fluorescence microscopy setup, we searched the literature to find a  
113 suitable ER single fluorophore-based GECI. This class of GECIs are intensimetric  $\text{Ca}^{2+}$  sensors,  
114 based on a circularly permuted fluorescent protein (e.g. GFP, YFP, or mApple) (Baird et al., 1999;  
115 Nakai et al., 2001; Zhao et al., 2011) fused at its C- and N-termini with the components of a  $\text{Ca}^{2+}$   
116 sensing module (i.e. CaM domain and the M13 peptide). In the presence of  $\text{Ca}^{2+}$ , this causes  
117 tightening of the interaction between C- and N-termini of the fluorophore, leading to increased  
118 brightness. *De facto*, this interaction induces an alteration of the spectral properties of the fluorescent  
119 protein with a strong increase in the fluorescence emitted (Nakai et al., 2001). Recently, de Juan-Sanz  
120 and colleagues (2017), generated two ER-localized, low-affinity  $\text{Ca}^{2+}$  variants of the intensimetric  
121 single fluorophore-based GECI GCaMP6 (Chen et al., 2013), dubbed ER-GCaMP6-150 and ER-  
122 GCaMP6-210 (where numbers indicate the *in vitro* Kd for  $\text{Ca}^{2+}$  of the two sensors expressed in  $\mu\text{M}$ )  
123 (de Juan-Sanz et al., 2017). Both sensors were found to be efficiently targeted to the ER lumen of  
124 animal cells and their sensitivity allowed the observation of a rapid  $\text{Ca}^{2+}$  accumulation in the axonal ER  
125 during an action potential firing (de Juan-Sanz et al., 2017). Remarkably, the two intensimetric  
126 GECIs, the ER-GCaMP3 variant and G-CEPIA1er, failed to reveal any signal in nerve terminals during  
127 activity, thus demonstrating a superior sensitivity of the ER-GCaMP6 sensors (de Juan-Sanz et al.,  
128 2017). Based on the fact that the CRT-D4ER, having an *in vitro* Kd for  $\text{Ca}^{2+}$  of 195  $\mu\text{M}$  (Palmer et al.,  
129 2006; Greotti et al., 2016), efficiently reports ER  $\text{Ca}^{2+}$  dynamics in plant cells (Bonza et al., 2013), we  
130 decided to test the ER-GCaMP6-210 variant to overcome the previous failures of other  $\text{Ca}^{2+}$  ER  
131 sensors in plants.

132 To express the ER-GCaMP6-210 sensor in plants, we generated different constructs (see Materials  
133 and Methods) by placing its coding sequence under the control of two different constitutive promoters  
134 (i.e. CaMV35S and pUBQ10) (Grefen et al., 2010; Amack and Antunes, 2020). The original ER-  
135 GCaMP6-210 harbours the signal peptide of calreticulin (CRT) at the N-terminus and the KDEL  
136 retention motif at the C-terminus which efficiently targeted the sensor to the ER of neuronal cells (de

137 Juan-Sanz et al., 2017). To verify that the N- and C-terminal sequences were also sufficient to localize  
138 the sensor to the ER of plant cells, we transiently co-expressed the two constructs in *Nicotiana*  
139 *benthamiana* leaf epidermal cells with the ER marker nWAK2-mCherry-HDEL (Nelson et al., 2007;  
140 Bonza et al., 2013) (**Supplemental Fig. S1**) The fluorescence emissions of ER-GCaMP6-210 and of  
141 the ER marker showed a clear merge in the cellular endomembrane system as well as in the NE  
142 (**Supplemental Fig. S1D, H, K**). The perfect merge of the two signals was particularly clear at higher  
143 magnifications (**Supplemental Fig. 11-K**). This experiment showed that the sensor was efficiently  
144 expressed under both promoters and that was properly localized to the ER (**Supplemental Fig. S1A,**  
145 **E**). When the ER-GCaMP6-210 was stably introduced in Arabidopsis Col-0 plants, the cellular  
146 fluorescence distribution was still clearly localized to the ER (Brandizzi et al., 2002; Bonza et al., 2013)  
147 and detected in both root and leaf cells (**Supplemental Fig. S2A-D**). Of note, the ER-GCaMP6-210  
148 was efficiently expressed in guard cells where a neat signal in the NE was recognized (**Supplemental**  
149 **Fig. S2G, I**). We tested the functionality of the new sensor in both pCaMV35S- and pUBQ10-ER-  
150 GCaMP6-210 Arabidopsis lines, challenging seedlings with external ATP (0.1 mM) as an efficient and  
151 reliable stimulus known to trigger a cytosolic  $\text{Ca}^{2+}$  concentration increase ( $[\text{Ca}^{2+}]_{\text{cyt}}$ ) in root-tip cells  
152 (Tanaka et al., 2010; Bonza et al., 2013; Behera et al., 2018). We performed parallel experiments  
153 using Arabidopsis seedlings expressing the cytosolic and nuclear-localized R-GECO1 sensor (Keinath  
154 et al., 2015). The first set of experiments were carried out following the same experimental design as  
155 that reported in Behera et al. (2018), where we made use of a custom perfusion setup for *in vivo* wide-  
156 field fluorescence microscopy imaging in Arabidopsis roots (Behera and Kudla, 2013). A 3-min pulsed  
157 ATP administration to the seedlings expressing ER-GCaMP6-210 and R-GECO1 triggered clear  
158 fluorescence increases which reflected a transient rise of  $[\text{Ca}^{2+}]_{\text{ER}}$  and  $[\text{Ca}^{2+}]_{\text{cyt}}$  (**Supplemental Fig.**  
159 **S3A**). The  $[\text{Ca}^{2+}]_{\text{ER}}$  peak (**Supplemental Fig. S3B**) temporally followed the  $[\text{Ca}^{2+}]_{\text{cyt}}$  rise  
160 (**Supplemental Fig. S3C**) and the ER showed a slower recovery to the prestimulus  $[\text{Ca}^{2+}]_{\text{ER}}$  compared  
161 to the  $[\text{Ca}^{2+}]_{\text{cyt}}$  (**Supplemental Fig. S3D**). Importantly, performing a comparison between seedlings  
162 expressing the ER-GCaMP6-210 with those expressing the Cameleon CRT-D4ER (Bonza et al.,



2013) revealed that the two sensors reported similar  $[Ca^{2+}]_{ER}$  dynamics in response to ATP, with no difference both in the times at which the  $[Ca^{2+}]_{ER}$  peak was reached (**Supplemental Fig. S3E, G**) and the times of recovery (**Supplemental Fig. S3H**). Instead, the ER-GCaMP6-210 exhibited a significantly increased signal change compared with the CRT-D4ER (**Supplemental Fig. S3F**). It has been reported that most of the single fluorescent protein GECIs show pH sensitivity (Zhao et al., 2011; Keinath et al., 2015). On the other hand, pH has a minor effect on the readout of ratiometric FRET-based sensors like Cameleon (Nagai et al., 2004; Behera et al., 2018; Grenzi et al., submitted). The high similarity of  $Ca^{2+}$  dynamics monitored by using the ER-GCaMP6-210 and CRT-D4ER suggests that in the ER lumen, the probable pH change, possibly dependent on a coupled  $Ca^{2+}/H^+$  transport occurring across the ER membrane (e.g. ECAs and ACAs exchange  $Ca^{2+}$  with  $H^+$  (Bonza and De Michelis, 2011; Resentini et al., 2021)), does not seem to affect the ER-GCaMP6-210 sensor readout. To further test the functionality of the ER-GCaMP6-210 sensor, we treated the seedlings (in both pCaMV35S- and pUBQ10 lines) with 0.01 mM naphthalene-1-acetic acid (NAA) (Behera et al., 2018). A 3-min pulsed NAA treatment was also efficient to induce a transient accumulation of  $Ca^{2+}$  in both compartments (**Supplemental Fig. S3I, J**), with the ER  $Ca^{2+}$  accumulation showing slower dynamics compared to the cytosol concerning both the maximum peak (**Supplemental Fig. S3K**) and the recovery of the prestimulus  $[Ca^{2+}]$  (**Supplemental Fig. S3L**).

Overall, whereas different ATP- and NAA-induced  $Ca^{2+}$  dynamics in the cytosol were well documented (Waadt et al., 2017; Behera et al., 2018), these new data showed that different dynamics were also detectable in the ER (**Supplemental Fig. S3A, I**). Specifically, in response to NAA the  $Ca^{2+}$  (expressed as  $\Delta F_{max}/F_0$ ) in the ER peak and the time when it was reached was smaller (e.g.  $0.37 \pm 0.11$  for NAA vs  $1.47 \pm 0.45$  for ATP with the pUBQ10-ER-GCaMP6-210 line) and delayed (e.g.  $157 \pm 32$  for NAA vs  $129.2 \pm 44$  for ATP with the pUBQ10-ER-GCaMP6-210 line), respectively, compared to the one measured with the ATP treatment (**Supplemental Fig. S3B, C, J, K**). Noticeably, this new set of results confirmed previously published data showing that the  $Ca^{2+}$  accumulation in the ER follows

188 the cytosolic  $\text{Ca}^{2+}$  transient, again supporting a role of ER as a  $\text{Ca}^{2+}$  sink in response to stimuli that  
189 induce a  $[\text{Ca}^{2+}]_{\text{cyt}}$  increase (Bonza et al., 2013, Corso et al., 2018).

190 Based on this first series of results, we felt confident that the ER-GCaMP6-210 sensor, despite the  
191 oxidative environment of the plant ER lumen (Aller et al., 2013) and the lower pH (Martinière et al.,  
192 2013), efficiently reports  $[\text{Ca}^{2+}]_{\text{ER}}$  dynamics in accordance with what was reported in animal neurons  
193 (de Juan-Sanz et al., 2017). Therefore, having demonstrated the functionality of the new sensor in  
194 monitoring ER  $\text{Ca}^{2+}$  dynamics, we explored the possibility of performing simultaneous imaging of  $\text{Ca}^{2+}$   
195 in ER and cytosol. To this end, we crossed both the pCaMV35S-ER-GCaMP6-210 and pUBQ10-ER-  
196 GCaMP6-210 Arabidopsis lines with the pUBQ10-R-GECO1 line (Zhao et al., 2011; Keinath et al.,  
197 2015) and selected seedlings showing both types of fluorescence (**Fig. 1A-D; Supplemental Fig. S4**).  
198 Since the stable expression of GECIs might affect plant growth and development (De Col et al., 2017;  
199 Waadt et al., 2017), before proceeding with further analyses we phenotypically characterized the  
200 Arabidopsis lines expressing the ER-GCaMP6-210 alone alongside those co-expressing the R-  
201 GECO1. We measured seedling root length, rosette size, silique length, and the number of seeds per  
202 silique of independent pCaMV35S-ER-GCaMP6-210, pUBQ10-ER-GCaMP6-210, and the R-GECO1  
203 crossed lines. By comparing these parameters with the Col-0 wild type, we did not observe any gross  
204 phenotypic differences in all sensor lines tested (**Supplemental Fig. S5A-D**), with only the  
205 pCaMV35S-ER-GCaMP6-210 line showing slightly reduced silique length and seed number  
206 (**Supplemental Fig. S5C, D**).

207 The proper expression of the ER-GCaMP6-210 under the control of the pUBQ10 promoter both alone  
208 (**Supplemental Fig. S2**) and co-expressed with the R-GECO1 (**Fig. 1A-D; Supplemental Fig. S4**),  
209 together with the lack of negative effects on plant growth and development (**Supplemental Fig. S5**),  
210 prompted us to choose the pUBQ10-ER-GCaMP6-210 x pUBQ10-R-GECO1 line to carry out the  
211 simultaneous imaging of  $\text{Ca}^{2+}$  dynamics in the two cellular compartments.

212 To prove the validity, usability, and advantages of this new dual biosensor line, we pursued two  
213 different approaches: i) high spatio-temporal resolution  $\text{Ca}^{2+}$  imaging analyses in single cells, and ii)  
214 low-magnification  $\text{Ca}^{2+}$  imaging analyses in adult mature plants.

215 Initially, we demonstrated the reliability of ATP and NAA to induce a transient  $\text{Ca}^{2+}$  accumulation in the  
216 cytosol and ER (**Supplemental Fig. S3**). Those experiments were carried out by means of a wide-  
217 field microscope which, given its poor optical sectioning, provides averaged responses on several  
218 root-tip cells (Costa et al., 2013; Vigani and Costa, 2019). To perform single-cell analyses in seedling  
219 root tips, we made use of a Spinning Disk confocal. We independently acquired the ER-GCaMP6-210  
220 and R-GECO1 fluorescence switching between GFP and RFP filters: the delay between the emissions  
221 was less than 600 ms and the images were acquired every 2 s (see Materials and Methods). For  
222 every experiment, we treated Arabidopsis root tips with 0.1 mM ATP or 0.01 mM NAA pulsed for 3 min  
223 using the same perfusion set up described above and we analyzed two different independent cell  
224 types (cell 1, C1, and cell 2, C2 in **Fig. 1**) (**Fig. 1E, L; Supplemental Movie S1**). Even at the single-  
225 cell level, the ER  $\text{Ca}^{2+}$  accumulation temporally followed the cytosolic increase (**Fig. 1F, G, M, N**),  
226 showing a delayed maximum peak and a slower recovery time (**Fig. 1H, J, K, O, Q, R**). It is  
227 noteworthy that the simultaneous imaging of the two compartments allowed us to precisely and  
228 directly determine the time delay between the beginning of the  $[\text{Ca}^{2+}]_{\text{cyt}}$  increase and the following  
229  $[\text{Ca}^{2+}]_{\text{ER}}$  accumulation. This delay turned out to be, for both treatments, around 4–5 s ( $4.8 \pm 2.2$  s for  
230 ATP and  $3.7 \pm 2.6$  for NAA) (**Fig. 1H, O**). Aside from the ability to report different ER  $\text{Ca}^{2+}$  dynamics in  
231 response to different stimuli, this approach allowed us to measure the time required by the ER to  
232 import  $\text{Ca}^{2+}$  in response to a cytosolic  $\text{Ca}^{2+}$  increase; thus, it represents an *in vivo* measurement of the  
233 activity of ER-localized  $\text{Ca}^{2+}$ -transporters (e.g. ER-localized ACAs and ECAs) (Bonza and De Michelis,  
234 2011). To assess *in vivo* the contribution of ECAs in the active import of  $\text{Ca}^{2+}$  into the ER lumen, and  
235 their impact on the cytosolic  $\text{Ca}^{2+}$  homeostasis, we used cyclopiazonic acid (CPA). CPA is a non-  
236 fluorescent inhibitor of SERCA-like  $\text{Ca}^{2+}$ -ATPases including plant P-Type IIA ECAs (Liang and Sze,  
237 1998). We treated Arabidopsis root tips of the dual sensor line with 25  $\mu\text{M}$  CPA pulsed for 3 min and

238 analyzed simultaneously in the same cell (**Fig. 2A, B**) both the  $[Ca^{2+}]_{ER}$  and  $[Ca^{2+}]_{cyt}$  dynamics (**Fig.**  
239 **2C**). Since we expected to have a CPA-dependent decrease in the ER-GCaMP6-210 fluorescence, to  
240 avoid bleaching of the sensor which might affect the measurement, we acquired images every 5 s  
241 instead of 2 s as for the experiments reported in Fig. 1. The CPA administration determined a quick  
242 and sustained decrease of ER-GCaMP6-210 fluorescence, indicative of an  $[Ca^{2+}]_{ER}$  depletion. The ER  
243  $Ca^{2+}$  depletion was followed by a transient increase of  $[Ca^{2+}]_{cyt}$  (**Fig. 2C**). The treatment with DMSO  
244 alone (used as a solvent for CPA) did not have any effect (dashed lines in **Fig. 2C'**), demonstrating  
245 that the observed response was specific to CPA treatment. Based on these data, we measured the  
246 time between the initial decrease of  $[Ca^{2+}]_{ER}$  and the increase in  $[Ca^{2+}]_{cyt}$  that was quantified in  $14 \pm 9$  s  
247 (**Fig. 2D, E**). Interestingly, the CPA washout did not allow the recovery of  $[Ca^{2+}]_{ER}$  indicating that once  
248 the inhibitor has entered the cell it cannot be quickly removed and that the ER-localized pumps are  
249 probably kept in an inactive state. Based on this latter result, we can claim that a decreased activity of  
250 the ECAs is sufficient to trigger a cytosolic  $Ca^{2+}$  increase (**Fig. 2F**), and thus that the ER can  
251 potentially work as a cytosolic  $Ca^{2+}$  source in signaling processes. At the same time, this experiment  
252 underlines the key role played by CPA-sensitive  $Ca^{2+}$  transporters for the maintenance of ER  $Ca^{2+}$   
253 homeostasis, confirming the data previously obtained with the CRT-D4ER line (Bonza et al., 2013).  
254 Nonetheless, this result demonstrates that other  $Ca^{2+}$  transporters such as the ACAs and  $Ca^{2+}$   
255 exchangers localized to the ER, tonoplast, and PM could be responsible for the observed recovery of  
256 the resting  $[Ca^{2+}]_{cyt}$  (Resentini et al., 2021).

257 We can, therefore, foresee that this new dual sensor line will constitute a useful tool to study *in planta*,  
258 and in different tissues or cell types at high spatio-temporal resolution, the ER/cytosolic  $Ca^{2+}$  handling  
259 in response to different stimuli, in different genetic backgrounds, or following pharmacological  
260 treatments.

261 Whereas the experiments carried out in root cells reported ER and cytosolic  $Ca^{2+}$  transients in  
262 response to the perception of an exogenously applied stimulus or following a pharmacological  
263 treatment, we also wanted to investigate the ER/cytosolic  $Ca^{2+}$  dynamics with single-cell resolution

264 during a developmental process, such as the pollen tube growth (Feijo et al., 2004), where a role of  
265 ER in the regulation of  $\text{Ca}^{2+}$  signaling has been suggested (Iwano et al., 2009, Barberini et al., 2018;  
266 Ishka et al., 2021). We collected pollen grains from flowers of the pUBQ10-ER-GCaMP6-210 x  
267 pUBQ10-R-GECO1 mature plants and let them germinate *in vitro* as previously described  
268 (Schoenaers et al., 2017). We visually inspected the germinated pollen grains and selected those  
269 showing both fluorescence signals. We then followed their *in vitro* growth, acquiring images every 2 s  
270 and measuring the fluorescence intensities of both sensors in a Region of Interest (ROI) "a" drawn in  
271 the tip region just underneath the clear zone (**Fig. 3A, B, G; Supplemental Movie S2A**). In ROI "a",  
272 the R-GECO1 revealed the typical tip cytosolic  $\text{Ca}^{2+}$  oscillations (**Fig. 3G, G'; Supplemental Movie**  
273 **S2A**) observed when pollens from different species germinate and grow *in vitro* (Damineli et al., 2017;  
274 Schoenaers et al., 2017; Barberini et al., 2018; Li et al., 2021). Pollen tubes showed a tip growth with  
275 an average speed of  $0.033 \pm 0.015 \mu\text{m/s}$  with cytosolic  $\text{Ca}^{2+}$  oscillations having an averaged frequency  
276 of  $0.03 \pm 0.01 \text{ Hz}$  (**Fig. 3G, G'**). These data are consistent with previous reports (Iwano et al., 2009,  
277 Damineli et al., 2017; Schoenaers et al., 2017) and confirm that, *in vitro*, the pollens did not have  
278 growth defects. This holds also true *in vivo* since no alterations were observed in silique length and  
279 seed number (**Supplemental Fig. S5C, D**). The ER-GCaMP6-210 fluorescence in the ROI "a" also  
280 showed an oscillating behaviour (**Fig. 3G, G'**), revealing the possible existence of  $[\text{Ca}^{2+}]_{\text{ER}}$  oscillations  
281 which might, therefore, correspond with the tip cytosolic  $\text{Ca}^{2+}$ , which is known to be dependent on an  
282 influx of extracellular  $\text{Ca}^{2+}$  (Holdaway-Clarke et al., 1997). To investigate this possibility, we performed  
283 a normalized cross-correlation analysis between the R-GECO1 and the ER-GCaMP6-210  
284 fluorescence signals. This analysis revealed a peak value of  $0.28 \pm 0.11$  (**Fig. 3H**) with a global  
285 temporal lag of  $6 \pm 2 \text{ s}$  (**Fig. 3I**) and an average oscillation time of  $30 \pm 11 \text{ s}$  (**Fig. 3J**), thus supporting  
286 a correlation between the two parameters. However, the combined effects of the continuous  
287 movement of the ER membranes, observed in the apex of the pollen tube (see the analyzed ROI "a"  
288 and the kymograph in **Fig. 3D**) (Lovy-Wheeler et al., 2007), and the intensimetric nature of the  
289 sensors do not make us confident to ascribe both the increase and decrease of the ER-GCaMP6-210

290 fluorescence uniquely to the sole change in the  $[Ca^{2+}]_{ER}$ . In this case, the use of a ratiometric sensor,  
291 such as the Cameleon CRT-D4ER, would probably help, but at present, we do not have a line  
292 expressing simultaneously the CRT-D4ER and the R-GECO1 in pollen. Nevertheless, the kymographs  
293 extracted for both fluorescence emissions of the representative pollen tube (**Fig. 3D-F**) revealed that  
294 an increase in the R-GECO1 and ER-GCaMP6-210 signals spread within the shank towards the grain  
295 (**Fig. 3D, K; Supplemental Movie S2B**), allowing us to quantify the R-GECO1 and ER-GCaMP6-210  
296 fluorescence emissions in a second ROI "b" drawn in a region of the pollen shank where the  
297 movement of the ER membranes was limited (**Fig. 3A, B, D, E**). Only a subpopulation of growing  
298 pollen tubes showed such cytosolic  $Ca^{2+}$  transients in the shank (ROI "b"), but when a change of R-  
299 GECO1 fluorescence was observed (**Fig. 3K, K'**), a clear increase of ER-GCaMP6-210 fluorescence  
300 was present, which followed the cytosolic signal with an average delay of  $3.2 \pm 1.1$  s (**Fig 3L**).  
301 Moreover, similar to what was observed in root-tip cells, the ER-GCaMP6-210 fluorescence showed a  
302 more sustained increase compared to the cytosolic one (**Fig. 3M**). Based on these observations, we  
303 suggest that the variation of ER-GCaMP6-210 fluorescence in the shank faithfully reported a change  
304 in the ER  $Ca^{2+}$  concentration and was not affected by heterogeneity in volume and concentration of  
305 the sensor.

306 In conclusion, although the ER-GCaMP6-210 allows efficient measurement of ER  $Ca^{2+}$  dynamics in  
307 pollen tubes, the data obtained by the analyses of the tip region should be taken with care.  
308 Nevertheless, we believe that this dual sensor line will be instrumental to re-evaluate, besides CPA,  
309 the action of a series of inhibitors, known to affect the ER  $Ca^{2+}$  release in animal cells (e.g. 2-  
310 aminoethoxydiphenyl borate, heparin, and caffeine), that have also been shown to impact the cytosolic  
311 tip  $Ca^{2+}$  gradient and growth of pollen tubes in different species (e.g. *Solanum lycopersicum*, *Papaver*  
312 *rhoeas*, *Nicotiana tabacum*) (Franklin-Tong et al., 1996; Barberini et al., 2018; Li et al., 2021).

313 The successful detection of single FP GECIs fluorescence (Vincent et al., 2017; Nguyen et al., 2018;  
314 Toyota et al., 2018) achieved with simple fluorescence microscopes (e.g. fluorescent  
315 stereomicroscopes) made us confident that this dual sensor line could also allow imaging of ER and

316 cytosolic  $\text{Ca}^{2+}$  dynamics in adult mature plants. Therefore, we imaged three-week-old Col-0 pUBQ10-  
317 ER-GCaMP6-210 x pUBQ10-R-GECO1 plants grown in soil, using a fluorescent stereomicroscope  
318 equipped with GFP and RFP filters (**Fig. 4A-C**). A rosette leaf was wounded by a tweezer according to  
319 Nguyen et al. (2018) and sensors' fluorescence emissions were monitored and quantified both in the  
320 wounded (local, l) and in a distal (d) leaf (**Fig. 4A-D**). The wounding induced both a cytosolic and ER  
321  $\text{Ca}^{2+}$  increase in the local leaf, occurring primarily in the vasculatures and spreading within the leaf  
322 lamina and the petiole, eventually reaching a distal leaf (**Fig. 4D-G; Supplemental Movie S3**). Note  
323 that the drop of the initial fluorescence signals for both sensors, detectable in the local and distal  
324 leaves, was due to the movement of the entire plant when touched with the tweezer (red arrow in **Fig.**  
325 **4F; Supplemental Movie S3**). Whereas the cytosolic  $\text{Ca}^{2+}$  increase was expected to occur both in the  
326 wounded leaf and in the distal one (Mousavi et al., 2013; Nguyen et al., 2018), the wounding-induced  
327 ER  $\text{Ca}^{2+}$  accumulation in both sites was a novel observation, demonstrating that the magnitude of the  
328 cytosolic  $\text{Ca}^{2+}$  increase (**Fig. 4H**) was sufficient to trigger the  $[\text{Ca}^{2+}]_{\text{ER}}$  accumulation. Similar to what  
329 was observed in the previous experiments, the  $[\text{Ca}^{2+}]_{\text{ER}}$  increase temporally followed the cytosolic one  
330 (**Fig. 4I**), being also more sustained (**Fig. 4F, G**). To further analyze the representative experiment, we  
331 visually represented the temporal progression of the cytosolic and ER  $\text{Ca}^{2+}$  accumulation (**Fig. 4L, M**)  
332 by using false colors, representing by each color the time at which the maximum intensity in  
333 fluorescence occurred. Pixel by pixel, the color was weighted by the absolute value achieved: the  
334 brighter the color, the higher the signal. Early signal peaks are labelled with blue color, fading to red  
335 and green for middle to late responses, respectively, thus presenting an overall idea about the signal  
336 propagation throughout the whole plant (**Fig. 4L, M**).

337 In conclusion, this latter result reports the existence of a long-distance ER  $\text{Ca}^{2+}$  wave induced by  
338 wounding that travels from leaf to leaf and temporally follows the cytosolic  $\text{Ca}^{2+}$  wave.

339

340 **CONCLUSIONS**

341 In this article, we report the generation of a new Arabidopsis line expressing both ER-GCaMP6-210  
342 and R-GECO1 GECIs for the simultaneous *in vivo* imaging of Ca<sup>2+</sup> dynamics in the ER and cytosol of  
343 plant cells. Our data confirm the critical role of the ER as a Ca<sup>2+</sup> buffering system and provide an  
344 unprecedented spatial and temporal resolution of the dynamics of [Ca<sup>2+</sup>]<sub>ER</sub> accumulation in different  
345 cell types in response to independent external stimuli and during a developmental program. This new  
346 technology allows us to demonstrate that, in response to leaf wounding, a long-distance ER Ca<sup>2+</sup> wave  
347 is established, which temporally follows the cytosolic one. This introduces an additional layer of  
348 complexity in the rapid long-range signaling in plants (Johns et al., 2021) and opens interesting new  
349 scenarios. The generation of this dual sensor line provides the basis for future experiments, feasible at  
350 any developmental stage, aimed at identifying critical components involved in the Ca<sup>2+</sup> transport  
351 across ER membranes of plant cells that are essential to shed more light on a still underappreciated  
352 role of this compartment in the regulation of local and systemic Ca<sup>2+</sup> signaling in plants.

353



## 354 MATERIALS AND METHODS

355 **Plant material and growth conditions.** All *Arabidopsis* (*Arabidopsis thaliana*) plants were of the  
356 ecotype Columbia 0 (Col-0). Seeds were surface-sterilized by vapor-phase sterilization (Clough and  
357 Bent, 1998) and plated on half-strength MS medium (Murashige and Skoog, 1962) (Duchefa,  
358 <http://www.duchefa-biochemie.com/>) supplemented with 0.1% (w/v) sucrose, 0.05% (w/v) MES, pH  
359 5.8, and 0.8% (w/v) plant agar (Duchefa, <http://www.duchefa-biochemie.com/>). After stratification at  
360 4°C in the dark for 2 days, plates were transferred to the growth chamber under long-day conditions  
361 (16 h light/8 h dark, 100  $\mu\text{E m}^{-2} \text{s}^{-1}$  of Cool White Neon lamps) at 22°C. The plates were kept vertically,  
362 and seedlings were used for imaging 6–7 days after germination (DAG). For imaging in adult plants,  
363 3–4-week-old mature plants grown in soil under long-day conditions (16 h light /8 h dark, 100  $\mu\text{E m}^{-2} \text{s}^{-1}$   
364 of Cool White Neon lamps) at 22°C and 75% relative humidity were used. *Nicotiana benthamiana*  
365 plants were cultivated for 5–6 weeks in a greenhouse under a 16-h light/8-h dark cycle with 60%  
366 atmospheric humidity and at 22/18°C.

367

368 **Plant phenotyping and root growth analyses.** For whole-plant phenotyping, plants were grown on  
369 soil under long-day conditions in individual pots randomly distributed among standard greenhouse  
370 flats. Rosettes and siliques were documented photographically. Seeds were harvested from individual  
371 siliques and counted. For phenotypic analysis on roots, surface-sterilized seeds were grown vertically  
372 on half-strength MS medium supplemented with 0.1% (w/v) sucrose, 0.8% (w/v) plant agar (Duchefa,  
373 <http://www.duchefa-biochemie.com/>), and root length was measured from 3 to 7 DAG. Lengths and  
374 sizes were quantified by Fiji (<https://imagej.net/Fiji>).

375

376 **Molecular cloning and plasmid constructs.** The original plasmid harboring the sequence coding for  
377 the ER-GCaMP6-210 (de Juan-Sanz et al., 2017) was obtained from Addgene  
378 (<https://www.addgene.org/86919/>). The *ER-GCaMP6-210* coding sequence was PCR amplified with

379 the Q5<sup>®</sup> High-Fidelity DNA Polymerase (New England Biolabs, <https://www.neb.com/>) using the  
380 following forward and reverse primers:

381 AC614 5'-CATGGGAATTCATGGGACTGCTGTCTGTGCCT-3' and

382 AC615 5'-CATGGGATCCTCACAGCTCATCCTTGCCTCC-3'

383 harboring the EcoRI and BamHI restrictions sites, respectively (underlined). The amplicon was ligated  
384 into the empty EcoRI/BamHI-digested *pGree0029-Ter* binary vector (Ter corresponds to the 19S  
385 CaMV terminator sequence) (Hellens et al., 2000; Bonza et al., 2013) to generate the *pGree0029-ER-*  
386 *GCaMP6-210-Ter*. pUBQ10 (Grefen et al., 2010) and pCaMV35S (Amack and Antunes, 2020)  
387 promoter sequences were amplified using the following primers:

388 AC280 5'-CATGGGTACCGTCGACGAGTCAGTAATAAACG-3';

389 AC281 5'-CATGGGTACCGTGTTAATCAGAAAACTCAG-3';

390 AC314 5'-CATGGGTACCGATATCGTACCCCTACTCCA-3' and

391 AC315 5'-CATGGGTACCGGGGCTGTCCTCTCCAAATGAA-3'.

392 All forward and reverse primers harbor a KpnI restriction site (underlined). The amplicons of both  
393 promoters were digested with KpnI and ligated into the KpnI-linearized and dephosphorylated  
394 *pGreen0029-ER-GCaMP6-210-Ter* plasmid. The obtained *pGreen0029-pUBQ10-ER-GCaMP6-210-*  
395 *Ter* and *pGreen0029-pCaMV35S-ER-GCaMP6-210-Ter* vectors were sequenced to verify the proper  
396 directionality of the inserted promoters and the absence of mistakes. The pGreen0029 vector  
397 backbone harbors the *nptII* gene, which confers the resistance to kanamycin in bacteria and the *nptII*  
398 gene which confers the resistance to kanamycin in plants (Hellens et al., 2000).

399

400 **Generation of transgenic plants.** The *pGreen0029-pUBQ10-ER-GCaMP6-210* and *pGreen0029-*  
401 *pCaMV35S-ER-GCaMP6-210* constructs were introduced in *Agrobacterium tumefaciens*  
402 *GV3101/pMMP90* strain. *Arabidopsis thaliana* Col-0 was transformed by floral-dip (Clough and Bent,

403 1998). Transgenic lines were selected by the presence of fluorescence for each construct. To obtain  
404 the double-sensor lines, the Col-0 pUBQ10-ER-GCaMP6-210 #1 and pCaMV35S-ER-GCaMP6-210  
405 #1 lines were crossed with the Col-0 pUBQ10-R-GECO1 line (Keinath et al., 2015).

406

407 **Transient expression in *Nicotiana benthamiana* leaves.** Leaf infiltration was performed using  
408 *Agrobacterium tumefaciens* GV3101/pMP90 strain carrying the specified constructs (pUBQ10-ER-  
409 GCaMP6-210-Ter; pCaMV35S-ER-GCaMP6-210-Ter, nWAK2-mCherry-HDEL) together with the p19-  
410 enhanced expression system according to the method described by Waadt and Kudla (2008). For the  
411 confocal imaging analysis after the infiltration, the plants were kept for 3–5 days under incubation  
412 conditions described above.

413

414 **Pollen tube growth dynamics.** To perform  $\text{Ca}^{2+}$  imaging analyses during pollen tube growth, pollen  
415 grains from 13–15 flowers-stage plants were germinated in accordance with Rodriguez-Enriquez et al.  
416 (2012) and Schoenaers et al. (2017) (292 mM sucrose, 0.16 mM  $\text{H}_3\text{BO}_3$ , 0.1 mM  $\text{CaCl}_2$ ; 0.14 mM  
417  $\text{Ca}(\text{NO}_3)_2$ ; 0.1 mM KCl, 0.003% (w/v) N-Z-Amine A; 0.055 mM myo-inositol, 0.038 mM ferric  
418 ammonium citrate; 0.01 mM spermidine; 10 mM gamma-Aminobutyric acid, pH 8.0 adjusted with KOH  
419 and 0.5% (w/v) agarose). The solution was heated in a microwave for the agarose to dissolve and  
420 cooled down to 50–60°C for the pH to be readjusted to pH 8.0. A 0.5 cm × 0.5 cm cellophane  
421 membrane (325P cellulose; AA Packaging Limited, Preston, United Kingdom) was placed on top of  
422 the medium, and pollen grains were placed directly onto the membrane, and the cover glass was  
423 flipped on another cover glass that was attached to an opening at the bottom of a small Petri dish.  
424 Water was applied on the inner sides of the Petri dish to maintain high humidity and the Petri dish was  
425 closed using parafilm. The pollen grains were germinated in a climate-controlled room at 23°C in the  
426 dark, and visualized approximately 2 h after pollination.

427

428 **Confocal laser scanning microscopy.** Confocal microscopy analyses of stable transgenic  
429 Arabidopsis seedling root and shoot cells and transiently transformed *N. benthamiana* leaf cells were  
430 performed using a Nikon Eclipse Ti2 inverted microscope, equipped with a Nikon A1R+ laser scanning  
431 device (<http://www.nikon.com/>). For localization studies, images were acquired by a CFI Apo Lambda  
432 40XC LWD WI (N.A. 1.15) and CFI Plan Apo Lambda 60X Oil (N.A. 1.4). ER-GCaMP6-210 was  
433 excited with the 488-nm laser and the emission was collected at 505–550 nm. R-GECO1 and mCherry  
434 were excited with the 561-nm laser and the emission was collected at 570–620 nm. Chlorophyll was  
435 excited with the 488-nm laser and the emission was collected at 663–738 nm. The confocal pinhole  
436 was set to 20.43  $\mu\text{m}$  and the images were acquired at 2048 x 2048 pixels resolution (**Fig. 1**). NIS-  
437 Elements (Nikon; <http://www.nis-elements.com/>) was used as a platform to control the microscope.  
438 Images in Figure 1 and Supplemental Figure 2A-C and G-I, were denoised by using the NIS-Element  
439 Denoise.ai plugin ([https://www.microscope.healthcare.nikon.com/en\\_EU/products/confocal-](https://www.microscope.healthcare.nikon.com/en_EU/products/confocal-microscopes/a1hd25-a1rhd25/nis-elements-ai)  
440 [microscopes/a1hd25-a1rhd25/nis-elements-ai](https://www.microscope.healthcare.nikon.com/en_EU/products/confocal-microscopes/a1hd25-a1rhd25/nis-elements-ai)). Non denoised images were analyzed using NIS-  
441 Elements and Fiji.

442

443 **Wide-field fluorescence microscopy.** For wide-field  $\text{Ca}^{2+}$  imaging analyses in seedling roots of  
444 pUBQ10-ER-GCaMP6-210, pCaMV35S-ER-GCaMP6-210, pUBQ10-R-GECO1, and pCaMV35S-  
445 CRT-D4ER lines, an inverted fluorescence Nikon microscope (Ti-E; <http://www.nikon.com/>) with a CFI  
446 Plan Apo VC 20X (N.A. 0.75) was used. Excitation light was produced by a fluorescent lamp (Prior  
447 Lumen 200 PRO; Prior Scientific; <http://www.prior.com>) set to 20% with 488 nm (470/40 nm) for the  
448 ER-GCaMP6-210 sensor, 561 nm (540/25 nm) for the R-GECO1, and 440 nm (436/20 nm) for CRT-  
449 D4ER. ER-GCaMP6-210 and R-GECO1 fluorescence emissions were collected at 505–530 nm and at  
450 576–626 nm respectively. For the analysis of the CRT-D4ER line, the FRET CFP/YFP optical block  
451 A11400-03 (emission 1, 483/32 nm for ECFP; emission 2, 542/27 nm for FRET/Citrine) with a dichroic  
452 510 nm mirror (Hamamatsu) was used. Images were collected with a Hamamatsu Dual CCD camera  
453 (ORCA-D2; <http://www.hamamatsu.com/>). Camera binning was set to 2 x 2 for the ER-GCaMP6-210

454 and R-GECO1, and to 4 x 4 for the CRT-D4ER. Exposure times (from 100 to 400 ms) were adjusted  
455 depending on the line analyzed. Images were acquired every 5 s. Filters and the dichroic mirrors were  
456 purchased from Chroma Technology (<http://www.chroma.com/>). NIS-Elements (Nikon; [http://www.nis-](http://www.nis-elements.com/)  
457 [elements.com/](http://www.nis-elements.com/)) was used as a platform to control the microscope, illuminator, and camera. Images  
458 were analyzed using Fiji.

459

460 **Spinning Disk Confocal Microscopy.** Confocal spinning disk microscopy analyses of root-tip cells  
461 and pollen tubes were performed using a Nikon Eclipse Ti2 inverted microscope, equipped with a  
462 Yokogawa Spinning Disk Confocal System  
([https://www.microscope.healthcare.nikon.com/en\\_EU/products/confocal-microscopes/csu-](https://www.microscope.healthcare.nikon.com/en_EU/products/confocal-microscopes/csu-series/specifications)  
464 series/specifications). The oil immersion CFI Plan Apo Lambda 60X Oil (N.A. 1.4) and the CFI Plan  
465 Apo VC 20X (N.A. 0.75) were used as objectives. ER-GCaMP6-210 was excited by a 488-nm single-  
466 mode optical fiber laser and the emission was collected at 525–550 nm. R-GECO1 was excited by a  
467 561-nm single-mode optical fiber laser and the emission was collected at 576–626 nm. Images were  
468 collected with a Photometrics Prime BSI CMOS camera ([http](http://www.photometrics.com/products/prime-family/primebsi/)  
469 [s://www.photometrics.com/products/prime-family/primebsi/](http://www.photometrics.com/products/prime-family/primebsi/)) with an exposure time of 200–300 ms with  
470 a 2 x 2 binning (1024 x 1024 pixels) for each emission.

471 For dynamic Ca<sup>2+</sup> imaging analyses, images were acquired every 2 s. The NIS-Element AR (Nikon,  
472 Japan, <http://www.nis-elements.com/>) was used as a platform to control the microscope, laser,  
473 camera, and post-acquisition analyses. Images in Figure 2 and 3 were denoised by using the NIS-  
474 Element Denoise.ai plugin ([https://www.microscope.healthcare.nikon.com/en\\_EU/products/confocal-](https://www.microscope.healthcare.nikon.com/en_EU/products/confocal-microscopes/a1hd25-a1rhd25/nis-elements-ai)  
475 [microscopes/a1hd25-a1rhd25/nis-elements-ai](https://www.microscope.healthcare.nikon.com/en_EU/products/confocal-microscopes/a1hd25-a1rhd25/nis-elements-ai)). Raw, non-denoised images were analysed using Fiji.

476

477 **Wound-induced calcium imaging in adult plants.** Adult plants of pUBQ10-ER-GCaMP6-210 x  
478 pUBQ10-R-GECO1 were imaged with a Nikon stereomicroscope (SMZ18, <http://www.nikon.com/>)

479 equipped with a 5.9 megapixel CMOS DS-Fi3 Microscope Camera. Excitation light was produced by a  
480 mercury light source (Intensilight; <http://www.nikon.com/>) with GFP and RFP filter Cubes. A Plan Apo  
481 0.5X objective was used without zoom for the imaging of the entire plant and images were collected  
482 with an exposure time of 1 s with a 2 x 2 camera binning (1440 x 1024 pixels) for each emission. R-  
483 GECO1 and ER-GCaMP6-210 images were acquired every 10 s by manually switching between the  
484 GFP and RFP configuration. During the entire experiment, plants were continuously illuminated.

485

486 **Seedling imaging.** Seven-day-old seedlings were used for root imaging. For root experiments,  
487 seedlings were kept in the growth chamber until the experiment and gently removed from the plate  
488 according to Behera and Kudla (2013), placed in the dedicated chambers and overlaid with cotton  
489 wool soaked in imaging solution (5 mM KCl, 10 mM MES, 10 mM CaCl<sub>2</sub> pH 5.8 adjusted with Tris-  
490 base). The root was continuously perfused with imaging solution using a perfusion pump (Behera et  
491 al., 2018) while the shoot was not submerged. Treatments were carried out by supplementing the  
492 imaging solution with 0.1 mM Na<sub>2</sub>ATP (sodium adenosine triphosphate) (from a 200 mM stock solution  
493 buffered at pH 7.4 with NaOH), 0.01 mM NAA (from a 10.74 mM stock solution) or 25 μM of CPA  
494 (from a 10 mM stock solution dissolved in 100 % (v/v) DMSO) administered for 3 min under  
495 continuous perfusion.

496

497 **Quantitative imaging analysis.** Fluorescence intensity was determined over regions of interest  
498 (ROIs), which corresponded to: i) cells of the meristematic and transition zone of seedling root tips  
499 (wide-field microscope); ii) single meristematic root-tip cells (spinning disk microscope); iii) pollen tube  
500 tip or shank (spinning disk microscope), and iv) wounded and unwounded leaves of adult plants  
501 (stereo microscope). ER-GCaMP6-210 and R-GECO1 emissions of the analyzed ROIs were used for  
502 single fluorescence emissions analyses. Citrine and ECFP emissions of CRT-D4ER of the analyzed  
503 ROIs were used for the ratio (R) calculation (Citrine/ECFP). Background subtraction was performed in

504 all experiments, except in those performed with adult plants imaged with the stereomicroscope.  
505 Fluorescence (F) and ratio (R) values at different time points were normalized to the initial  
506 fluorescence ( $F_0$ ) ( $\Delta F/F_0$ ) or ratio ( $R_0$ ) ( $\Delta R/R_0$ ) and plotted versus time. For pollen experiments, the  
507 fluorescence emissions were normalized as  $(X - \text{mean})/SD$ . Where X is the fluorescence value at a  
508 given time point, mean and SD are respectively the average fluorescence value of all the time points  
509 and the associated standard deviation. The analysis of fluorescent intensities was in all cases  
510 performed on raw non-denoised images.

511

512 **Pollen tubes registration and growth analysis.** To quantify the tip  $\text{Ca}^{2+}$  oscillations in pollen tubes,  
513 we applied a semi-automatic routine to register the image stacks taken at different times. The  
514 registration of each ROI was performed by computing the cross-correlation between each couple of  
515 consecutive images. In this way, the pollen tube apex was maintained at the same position. This  
516 computation was performed with the Fiji plugin 'Template Matching'  
517 (<https://sites.google.com/site/qingzongtseng/template-matching-ij-plugin>) after selecting the pollen  
518 tube apex as a landmark and using a subpixel cross-correlation method. The horizontal and vertical  
519 displacements were stored, and the process was iterated for all time points. The average speed of the  
520 pollen tube growth was obtained by dividing the total elongation by the time.

521

522 **Kymograph.** To evaluate the pollen tube elongation, we used a graphical method for a space-time  
523 representation of the pollen tube tip evolution. We draw a spatial path that follows the tip of the tube  
524 during its growth, as observed in the entire image sequence (x,y,t). By using the Fiji "Dynamic Reslice"  
525 function we create a new image, which depicts the temporal evolution of the pollen elongation through  
526 the spatial path previously defined.

527

528 **Cross-correlation analyses of fast fluctuations.** To evaluate the temporal delay between the two  
529 fluorescent channels, we performed a signal analysis based on cross-correlation. To understand the  
530 correlation between the fast oscillations occurring in both the R-GECO1 and ER-GCaMP6-210, we  
531 used a statistical approach based on the data acquired in the set of 9 independent measurements.  
532 First, we removed the slow dynamics in each signal, estimated by subtracting a low-pass version of  
533 the temporal signature. Such a low-pass version was obtained by filtering the signal with a gaussian  
534 kernel of sigma  $\sigma = 80$  s. Consecutively, each curve obtained was examined by running cross-  
535 correlation analysis in sliding windows of 80 s, with a stride of 2 s. Within each temporal window, we  
536 normalized the signal by its standard deviation and subtracted the mean. In this way, we could  
537 calculate the normalized version of the cross-correlation. This analysis was repeated by striding the  
538 window through the entire signal duration for all the measurements and let us estimate the average  
539 cross-correlation and its associated error. The temporal location of the peaks indicates an average  
540 temporal delay between the two signals.

541

542 **Temporal representation of  $\text{Ca}^{2+}$  waves in mature plants.** To produce a visual representation of the  
543 overall temporal propagation of the  $\text{Ca}^{2+}$  signals in the whole plant, we first removed a common  
544 background in the images, segmenting the plant (by thresholding) and setting to zero the values  
545 outside of the plant. We then realigned each time point of the same leaf by selecting a region that  
546 enclosed it. In the successive frames, we compensated for the movement by evaluating the cross-  
547 correlation displacement. In this way, the intensity in each pixel described the temporal evolution of  
548 the signal in a given position within the leaf. Once each leaf was spatially realigned for the entire  
549 duration of the acquisition, it was possible to compute the  $\Delta F/F_0$  on the full image sequence. To obtain  
550 a visual image that describes the temporal propagation by using a false-color representation, we  
551 mapped the temporal location of the maximum intensity in each pixel with a color in the look-up table.  
552 The color intensity was chosen to be proportional to the peak intensity found in the temporal evolution



553 of the pixel. In this representation, the blue color indicates that the peak intensity was achieved at  
554 early timings, fading to red and green for middle and late timings.

555

556 **Statistical analysis.** All the data are representative of  $n \geq 4$  experiments. Reported traces are  
557 averages of traces from all single experiments used for the statistical analyses. Results are reported  
558 as averages  $\pm$  standard deviations (SD).  $p$  values were calculated with an unpaired Student's  $t$ -test.  
559 Data from experiments with at least  $n = 5$  were plotted as box-and-whisker plots using GraphPad, in  
560 which all the experimental points are plotted, and their distribution represented as a box that extends  
561 from the 25<sup>th</sup> to 75<sup>th</sup> percentiles. The line in the middle of the box is plotted at the median.

562

563

#### 564 **SUPPLEMENTAL DATA**

565 **Supplemental Figure S1.** Subcellular distribution of ER-GCaMP6-210 in *N. benthamiana* leaf  
566 epidermal cells.

567 **Supplemental Figure S2.** Confocal microscopy analyses revealed efficient ER-GCaMP6-210  
568 expression in different organs of Arabidopsis stable transgenic pUBQ10-ER-GCaMP6-210.

569 **Supplemental Figure S3.** Cytosolic and ER  $Ca^{2+}$  transients in root-tip cells of Arabidopsis seedlings  
570 expressing the R-GECO1 (cytosolic and nuclear localized) and ER-GCaMP6-210 (ER localized)  
571 sensors in response to external ATP (0.1 mM) and NAA (0.01 mM), and Cameleon CRT-D4ER (ER  
572 localized) in response to external ATP (0.1 mM).

573 **Supplemental Figure S4.** Co-expression of ER-GCaMP6-210 and R-GECO1 in guard cells.

574 **Supplemental Figure S5.** Plant development is unchanged in the generated calcium indicators lines.

575 **Supplemental Movie S1.** Movie from a representative time series of a wt Arabidopsis seedling root tip  
576 expressing the ER-GCaMP6-210 (green) and R-GECO1 (magenta) sensors in response to external  
577 ATP. Scale bar 15  $\mu\text{m}$ .

578 **Supplemental Movie S2.** Movie from two representative time series of wt Arabidopsis pollen tubes  
579 expressing the ER-GCaMP6-210 (green) and R-GECO1 (magenta) sensors. Scale bar 20  $\mu\text{m}$ .

580 **Supplemental Movie S3.** Movie from a representative time series of a wt Arabidopsis mature plant  
581 expressing the ER-GCaMP6-210 (green) and R-GECO1 (magenta) sensors in response to leaf  
582 wounding. Scale bar 1 mm.

583

584 **ACKNOWLEDGMENTS**

585 We thank Dr. Melanie Krebs (University of Heidelberg) for providing us the pUBQ10-R-GECO1  
586 Arabidopsis line, and Prof. Kris Visseberg and Dr. Sébastien Schoenaers (University of Antwerp) for  
587 their training in the pollen tube growth assays. This work was supported by Piano di Sviluppo di  
588 Ateneo 2019 (University of Milan) (to AC), by Ministero dell'Istruzione, dell'Università e della Ricerca  
589 Fondo per Progetti di ricerca di Rilevante Interesse Nazionale 2017 (PRIN 2017ZBBYNC) (to MCB),  
590 and by a PhD fellowship from the University of Milan (to MG). We acknowledge fundings from H2020  
591 Marie Skłodowska-Curie Actions (HI-PHRET project, 799230) (to DA). Imaging analyses were carried  
592 out at NOLIMITS, an advanced imaging facility established by the University of Milan. Plant  
593 transformation and selection were supported by the "Piattaforma Piante" from the Department of  
594 Biosciences at the University of Milan.

595

596 **COMPETING INTERESTS**

597 The authors have declared that no competing interests exist.

598

599 **FIGURE LEGENDS:**

600 **Figure 1.** Simultaneous cytosolic and ER  $\text{Ca}^{2+}$  analyses in root tip at the single-cell level. **(A-D)**  
601 Images of root-tip cells of a representative pUBQ10-ER-GCaMP6-210 x pUBQ10-R-GECO1 seedling.  
602 **(A)** Green: ER-GCaMP6-210 fluorescence. **(B)** Magenta: R-GECO1 fluorescence. **(C)** Overlay of (A)  
603 and (B). Scale bar 25  $\mu\text{m}$ . **(D)** Lower magnification image of (C). Scale bar 50  $\mu\text{m}$ . **(E)** Exemplary  
604 false-color images illustrate R-GECO1 (magenta) and ER-GCaMP6-210 (green) of cell 1 (C1) and cell  
605 2 (C1) in root tips of seedlings expressing simultaneously the two  $\text{Ca}^{2+}$  sensors at steady-state and  
606 during the  $\text{Ca}^{2+}$  transient induced by the treatment with 0.1 mM ATP for 3 min. **(F)** R-GECO1 and ER-  
607 GCaMP6-210 normalized fluorescence changes of C1 over the time acquired under continuous  
608 perfusion and treated with 0.1 mM ATP for 3 min, as indicated by the black box on the x-axis. **(F')**  
609 same as panel (F) but x-axis, y-axis scales, and ranges adjusted. **(G)** R-GECO1 and ER-GCaMP6-  
610 210 normalized fluorescence changes of C2 over the time acquired under continuous perfusion and  
611 treated with 0.1 mM ATP for 3 min, as indicated by the black box on the x-axis. **(G')** same as panel (G)  
612 but x-axis, y-axis scales, and ranges adjusted. The double arrow in (F') and (G') indicates the delay  
613 time quantified in (H). **(H)** Mean delay of the fluorescence increase of the ER-GCaMP6-210 compared  
614 to the fluorescence change of the R-GECO1 for C1 and C2 following 0.1 mM ATP administration. **(I)**  
615 Maximal peaks of ER-GCaMP6-210 and R-GECO1 fluorescence signals for C1 and C2 after 0.1 mM  
616 ATP administration. **(J)** Time required to reach maximal peaks of ER-GCaMP6-210 and R-GECO1  
617 fluorescence emissions for C1 and C2 after stimulus administration. **(K)** Time required to pass half-  
618 maximal ER-GCaMP6-210 and R-GECO1 fluorescence signals during recovery after the stimulus.  $n =$   
619 7. **(L)** Exemplary false-color images illustrate R-GECO1 (magenta) and ER-GCaMP6-210 (green) of  
620 C1 and C2 in root tips of seedlings expressing simultaneously the two  $\text{Ca}^{2+}$  sensors, at steady-state  
621 and during the  $\text{Ca}^{2+}$  increase induced by the treatment with 0.01 mM NAA for 3 min. **(M)** R-GECO1  
622 and ER-GCaMP6-210 normalized fluorescence changes of C1 over the time acquired under  
623 continuous perfusion and treated with 0.01 mM NAA for 3 min, as indicated by the black box on the x-  
624 axis. **(M')** same as panel (M) but x-axis, y-axis scales, and ranges adjusted. **(N)** R-GECO1 and ER-

625 GCaMP6-210 normalized fluorescence changes of C2 over the time acquired under continuous  
 626 perfusion and treated with 0.01 mM NAA for 3 min, as indicated by the black box on the x-axis. **(N')**  
 627 same as panel (N) but x-axis, y-axis scales, and ranges adjusted. The double arrow in (M') and (N')  
 628 indicates the delay time quantified in (O). **(O)** Mean delay of the fluorescence increase of the ER-  
 629 GCaMP6-210 compared to the fluorescence change of the R-GECO1 for C1 and C2 following 0.01  
 630 mM NAA administration. **(P)** Maximal peaks of ER-GCaMP6-210 and R-GECO1 fluorescence signals  
 631 for C1 and C2 after 0.01 mM NAA administration. **(Q)** Time required to reach maximal peaks of ER-  
 632 GCaMP6-210 and R-GECO1 fluorescence signals for C1 and C2 after stimulus administration. **(R)**  
 633 Time required to pass half-maximal ER-GCaMP6-210 and R-GECO1 fluorescence emissions during  
 634 recovery after the stimulus.  $n = 6$ . Error bars = SD, ns = not significant, \* $p \leq 0.05$ , \*\* $p \leq 0.005$ , \*\*\* $p \leq$   
 635 0.0005 (Student's *t*-test).

636

637 **Figure 2.** Simultaneous cytosolic and ER  $\text{Ca}^{2+}$  analyses in root-tip cells treated with the P-Type IIA  
 638 inhibitor cyclopiazonic acid (CPA). **(A)** Green: ER-GCaMP6-210 fluorescence, Magenta: R-GECO1  
 639 fluorescence, and overlay. Scale bar 50  $\mu\text{m}$ . **(B)** Examples of false-color images illustrate R-GECO1  
 640 (magenta) and ER-GCaMP6-210 (green) of the selected cell (dashed rectangle in (A)) in root tips of  
 641 seedlings expressing simultaneously the two  $\text{Ca}^{2+}$  sensors at steady-state and during the  $\text{Ca}^{2+}$   
 642 treatment with 25  $\mu\text{M}$  CPA for 3 min. **(C)** R-GECO1 and ER-GCaMP6-210 normalized fluorescence  
 643 changes of the selected cell over the time acquired under continuous perfusion and treated with 25  $\mu\text{M}$   
 644 CPA for 3 min, as indicated by the black box on the x-axis. **(C')** R-GECO1 and ER-GCaMP6-210  
 645 normalized fluorescence of the selected cell over the time acquired under continuous perfusion and  
 646 treated with DMSO (the CPA solvent) as a control for 3 min, as indicated by the black box on the x-  
 647 axis. **(D)** same as panel (C) but x-axis, y-axis scales, and ranges adjusted. The double arrow in (D)  
 648 indicates the delay time quantified in (E). **(E)** Mean delay of the fluorescence increase of the R-  
 649 GECO1 following the ER-GCaMP6-210 fluorescence decrease. **(F)** The maximal peak of R-GECO1

650 and the minimal level of ER-GCaMP6-210 fluorescence signals for the selected cells after CPA  
 651 administration.  $n = 5$ . Error bars = SD.

652

653 **Figure 3.** Simultaneous ER-GCaMP6-210 and R-GECO1 fluorescence signals in growing pollen  
 654 tubes. **(A-C)** Images of a representative pollen tube. **(A)** Green: ER-GCaMP6-210 fluorescence. **(B)**  
 655 Magenta: R-GECO1 fluorescence. **(C)** Overlay of (A) and (B). Scale bar 20  $\mu\text{m}$ . **(D-F)** Kymograph  
 656 extracted from both fluorescence signals frames by observing the temporal evolution of the pixel line  
 657 highlighted in yellow. **(D)** Kymograph of 1200 s acquisitions extracted for the R-GECO1 images. **(E)**  
 658 Kymograph of 1200 s acquisitions extracted for the ER-GCaMP6-210 images. **(F)** Overlay of (D) and  
 659 (E). (a) = selected ROI for analyses of pollen tube tip fluorescence signals. (b) selected ROI for  
 660 analyses of pollen tube shank fluorescence signals. **(G)** Representative oscillations of ER-GCaMP6-  
 661 210 and R-GECO1 fluorescences in the tip (ROI “a”). **(G’)** same as panel (G) but x-axis, y-axis scales,  
 662 and ranges adjusted. **(H)** Normalized cross-correlation analysis between R-GECO1 and ER-GCaMP6-  
 663 210 averaged in temporal sliding windows of 80 s over  $n = 9$  measurements. The peak-value is  $0.28 \pm$   
 664  $0.11$ , and it is reached at positive delays, implying that the fast oscillations in the cytosol (R-GECO1)  
 665 are anticipated by the ones in the ER (ER-GCaMP6-210). **(I)** Distribution of the average delays by  
 666 locating in time the maximum of the cross-correlations, for each experiment considered. The global  
 667 temporal lag is  $6 \pm 2$  s. **(J)** Distribution of the period of the fast oscillations in the ER/Cytosol. It is  
 668 defined by doubling the temporal distance at which the signals correlate (maximum in G) and anti-  
 669 correlates (minimum). The average is  $30 \pm 11$  s. **(K)** Representative ER-GCaMP6-210 and R-GECO1  
 670 fluorescences in the shank (ROI “b”). **(K’)** same as panel (K) but x-axis, y-axis scales and ranges  
 671 adjusted. The double arrow in (K’) indicates the delay time quantified in (L). **(L)** Mean delay of the  
 672 fluorescence increase of the ER-GCaMP6-210 compared to the fluorescence change of the R-  
 673 GECO1. **(M)** Time required to pass half-maximal ER-GCaMP6-210 and R-GECO1 fluorescence  
 674 emissions during recovery after the spike.  $n = 5$ . Error bars = SD,  $*p \leq 0.05$  (Student’s *t*-test).

676 **Figure 4.** Simultaneous cytosolic and ER  $\text{Ca}^{2+}$  analyses in leaves of adult plants challenged with leaf  
 677 wounding. **(A-C)** Images of a representative pUBQ10-ER-GCaMP6-210 x pUBQ10-R-GECO1 mature  
 678 plant. **(A)** Green: ER-GCaMP6-210 fluorescence. **(B)** Magenta: R-GECO1 fluorescence. **(C)** Overlay  
 679 of (A) and (B). Scale bar 1 mm. **(D)** Examples of false-color images illustrate R-GECO1 (magenta) and  
 680 ER-GCaMP6-210 (green) in a local wounded leaf ("l"). **(F)** R-GECO1 and ER-GCaMP6-210  
 681 normalized fluorescence changes of the local leaf ("l") over the time after its wounding (red arrow). **(E)**  
 682 Examples of false-color images illustrate R-GECO1 (magenta) and ER-GCaMP6-210 (green) of a  
 683 distal leaf of the same wounded plant of (D). **(G)** R-GECO1 and ER-GCaMP6-210 normalized  
 684 fluorescence changes of a distal leaf ("d") over the time after wounding of "l". **(H)** Maximal peaks of  
 685 ER-GCaMP6-210 and R-GECO1 fluorescence signals in the local and distal leaves after wounding. **(I)**  
 686 Time required to reach maximal peaks of ER-GCaMP6-210 and R-GECO1 fluorescence signals in the  
 687 local and distal leaves after wounding.  $n = 5$ . **(L-M)** Digitally extracted images of a representative  
 688 pUBQ10-ER-GCaMP6-210 x pUBQ10-R-GECO1 plant for comparative analyses of the temporal  
 689 evolution of  $\text{Ca}^{2+}$  dynamics in the cytosol and ER compartments in response to leaf wounding. **(L)**  
 690 Temporal analysis of the  $\Delta F/F_0$  signal peak in the leaves for the R-GECO1. The temporal window  
 691 analyzed is of 750 s. The color-bar encodes the time at which the maximum signal is recorded in each  
 692 pixel. The wounded leaf is colored with blue, since it peaks at around 30 s. The distal leaf is reddish  
 693 because the maximum signal happens at 500 s. The other two leaves showed a delayed response, at  
 694 750 s. **(M)** Same analysis for the ER-GCaMP6-210 as in (L). The wounded leaf responded earlier (200  
 695 s, violet) than the distal one (750 s, green). Error bars = SD, \* $p \leq 0.05$ , \*\* $p \leq 0.005$  (Student's  $t$ -test).

696 **REFERENCES**

- 697 **Aller I, Rouhier N, Meyer AJ** (2013) Development of roGFP2-derived redox probes for measurement  
698 of the glutathione redox potential in the cytosol of severely glutathione-deficient *rml1* seedlings. *Front*  
699 *Plant Sci* **16**;4:506.
- 700 **Amack SC, Antunes MS** (2020) CaMV35S promoter – A plant biology and biotechnology workhorse  
701 in the era of synthetic biology. *Curr Plant Biol* **24**: 100179
- 702 **Baird GS, Zacharias DA, Tsien RY** (1999) Circular permutation and receptor insertion within green  
703 fluorescent proteins. *Proc Natl Acad Sci USA* **96**: 11241-11246
- 704 **Barberini ML, Sigaut L, Huang W, Mangano S, Juarez SPD, Marzol E, Estevez J, Obertello M,**  
705 **Pietrasanta L, Tang W, Muschietti J** (2018) Calcium dynamics in tomato pollen tubes using the  
706 Yellow Cameleon 3.6 sensor. *Plant Reprod* **31**:159-169
- 707 **Behera S, Kudla J** (2013) High-resolution imaging of cytoplasmic Ca<sup>2+</sup> dynamics in Arabidopsis roots.  
708 *Cold Spring Harb Protoc* 2013: 665-669
- 709 **Behera S, Xu Z, Luoni L, Bonza MC, Doccu FG, De Michelis MI, Morris RJ, Schwarzländer M,**  
710 **Costa A** (2018) Cellular Ca<sup>2+</sup> Signals Generate Defined pH Signatures in Plants. *Plant Cell* **30**: 2704-  
711 2719
- 712 **Bonza, M.C., De Michelis, M.I.** (2011). The plant Ca<sup>2+</sup>-ATPase repertoire: biochemical features and  
713 physiological functions. *Plant Biol.* **13**: 421-430
- 714 **Bonza, M.C., Loro, G., Behera, S., Wong, A., Kudla, J., Costa, A.** (2013). Analyses of Ca<sup>2+</sup>  
715 accumulation and dynamics in the endoplasmic reticulum of Arabidopsis root cells using a genetically  
716 encoded Cameleon sensor. *Plant Physiol.* **163**: 1230-1241
- 717 **Brandizzi F, Fricker M, Hawes C** (2002) A greener world: the revolution in plant bioimaging. *Nat Rev*  
718 *Mol Cell Biol* **3**: 520-530
- 719 **Charpentier M, Sun J, Vaz Martins T, Radhakrishnan GV, Findlay K, Soumpourou E, Thouin J,**



720 **Very AA, Sanders D, Morris RJ, Oldroyd GE** (2016) Nuclear-localized cyclic nucleotide-gated  
721 channels mediate symbiotic calcium oscillations. *Science* **352**: 1102-1105

722 **Chen TW, Wardill TJ, Sun Y, Pulver SR, Renninger SL, Baohan A, Schreiter ER, Kerr RA, Orger**  
723 **MB, Jayaraman V, Looger LL, Svoboda K, Kim DS** (2013) Ultrasensitive fluorescent proteins for  
724 imaging neuronal activity. *Nature* **499**: 295-300

725 **Clough SJ, Bent AF** (1998) Floral dip: a simplified method for *Agrobacterium*-mediated  
726 transformation of *Arabidopsis thaliana*. *Plant J* **16**: 735-743

727 **Corso M, Doccua FG, de Melo JRF, Costa A, Verbruggen N** (2018) Endoplasmic reticulum-  
728 localized CCX2 is required for osmotolerance by regulating ER and cytosolic Ca<sup>2+</sup> dynamics in  
729 *Arabidopsis*. *Proc Natl Acad Sci USA* **115**: 3966-3971

730 **Costa A, Candeo A, Fieramonti L, Valentini G, Bassi A** (2013) Calcium dynamics in root cells of  
731 *Arabidopsis thaliana* visualized with selective plane illumination microscopy. *PLoS One*  
732 **16**;8(10):e75646.

733 **Damineli DSC, Portes MT, Feijó JA** (2017) Oscillatory signatures underlie growth regimes in  
734 *Arabidopsis* pollen tubes: computational methods to estimate tip location, periodicity, and  
735 synchronization in growing cells. *J Exp Bot* **68**: 3267-3281

736 **De Col V, Fuchs P, Nietzel T, Elsässer M, Voon CP, Candeo A, Seeliger I, Fricker MD, Grefen C,**  
737 **Møller IM, Bassi A, Lim BL, Zancani M, Meyer AJ, Costa A, Wagner S, Schwarzländer M** (2017)  
738 ATP sensing in living plant cells reveals tissue gradients and stress dynamics of energy physiology.  
739 *Elife* **18**;6:e26770

740 **de Juan-Sanz J, Holt GT, Schreiter ER, de Juan F, Kim DS, Ryan TA** (2017) Axonal endoplasmic  
741 reticulum Ca<sup>2+</sup> content controls release probability in CNS nerve terminals. *Neuron* **93**: 867-881

742 **Edel KH, Marchadier E, Brownlee C, Kudla J, Hetherington AM** (2017) The evolution of calcium-  
743 based signalling in plants. *Curr Biol* **27**: R667-r679

- 744 **Feijó JA, Costa SS, Prado AM, Becker JD, Certal AC** (2004) Signalling by tips. *Curr Opin Plant Biol*  
745 **7**: 589-598
- 746 **Foskett JK, White C, Cheung KH, Mak DO** (2007) Inositol trisphosphate receptor  $Ca^{2+}$  release  
747 channels. *Physiol Rev* **87**: 593-658
- 748 **Franklin-Tong VE, Drobak BK, Allan AC, Watkins P, Trewavas AJ** (1996) Growth of pollen tubes of  
749 *Papaver rhoeas* is regulated by a slow-moving calcium wave propagated by inositol 1,4,5-  
750 trisphosphate. *Plant Cell* **8**: 1305-1321
- 751 **Grefen C, Donald N, Hashimoto K, Kudla J, Schumacher K, Blatt MR** (2010) A ubiquitin-10  
752 promoter-based vector set for fluorescent protein tagging facilitates temporal stability and native  
753 protein distribution in transient and stable expression studies. *Plant J* **64**: 355-365
- 754 **Greotti E, Wong A, Pozzan T, Pendin D, Pizzo P** (2016) Characterization of the ER-Targeted Low  
755 Affinity  $Ca^{2+}$  Probe D4ER. *Sensors (Basel)*. **16**(9):1419
- 756 **Hellens RP, Edwards EA, Leyland NR, Bean S, Mullineaux PM** (2000) pGreen: a versatile and  
757 flexible binary Ti vector for *Agrobacterium*-mediated plant transformation. *Plant Mol Biol* **42**: 819-832
- 758 **Holdaway-Clarke TL, Feijo JA, Hackett GR, Kunkel JG, Hepler PK** (1997) Pollen tube growth and  
759 the intracellular cytosolic calcium gradient oscillate in phase while extracellular calcium influx is  
760 delayed. *Plant Cell* **9**: 1999-2010
- 761 **Iwano M, Entani T, Shiba H, Kakita M, Nagai T, Mizuno H, Miyawaki A, Shoji T, Kubo K, Isogai A,**  
762 **Takayama S** (2009) Fine-tuning of the cytoplasmic  $Ca^{2+}$  concentration is essential for pollen tube  
763 growth. *Plant Physiol* **150**: 1322-1334
- 764 **Ishka MR, Brown E, Rosenberg A, Romanowsky S, Davis J, Choi W-G, Harper JF** (2021)  
765 *Arabidopsis*  $Ca^{2+}$ -ATPases 1, 2, and 7 in the endoplasmic reticulum contribute to growth and pollen  
766 fitness. *Plant Physiol* doi.org/10.1093/plphys/kiab021
- 767 **Johns S, Hagihara T, Toyota M, Gilroy S** (2021) The Fast and The Furious: Rapid long-range

768 signaling in plants. *Plant Physiol* doi.org/10.1093/plphys/kiaa098

769 **Keinath NF, Waadt R, Brugman R, Schroeder JI, Grossmann G, Schumacher K, Krebs M** (2015)  
770 Live cell imaging with R-GECO1 sheds light on flg22- and chitin-induced transient  $[Ca^{2+}]_{cyt}$  patterns in  
771 *Arabidopsis*. *Mol Plant* **8**: 1188-1200

772 **Leitão N, Dangeville P, Carter R, Charpentier M** (2019) Nuclear calcium signatures are associated  
773 with root development. *Nat Commun* **25**:10(1):4865

774 **Li K, Prada J, Damineli DSC, Liese A, Romeis T, Dandekar T, Feijó JA, Hedrich R, Konrad KR**  
775 (2021) An optimized genetically encoded dual reporter for simultaneous ratio imaging of  $Ca^{2+}$  and  $H^+$   
776 reveals new insights into ion signaling in plants. *New Phytol* doi: 10.1111/nph.17202.

777 **Liang F, Sze H** (1998) A high-affinity  $Ca^{2+}$  pump, ECA1, from the endoplasmic reticulum is inhibited  
778 by cyclopiazonic acid but not by thapsigargin. *Plant Physiol* **118**: 817-825

779 **Lovy-Wheeler A, Cárdenas L, Kunkel JG, Hepler PK** (2007) Differential organelle movement on the  
780 actin cytoskeleton in lily pollen tubes. *Cell Motil Cytoskeleton* **64**: 217-232

781 **Luo J, Chen L, Huang F, Gao P, Zhao H, Wang Y, Han S** (2020) Intraorganellar calcium imaging in  
782 *Arabidopsis* seedling roots using the GCaMP variants GCaMP6m and R-CEPIA1er. *J Plant Physiol*  
783 **246-247**:153127

784 **Martinière A, Bassil E, Jublanc E, Alcon C, Reguera M, Sentenac H, Blumwald E, Paris N** (2013)  
785 *In vivo* intracellular pH measurements in tobacco and *Arabidopsis* reveal an unexpected pH gradient  
786 in the endomembrane system. *Plant Cell* **25**: 4028-4043

787 **Mousavi SA, Chauvin A, Pascaud F, Kellenberger S, Farmer EE** (2013) GLUTAMATE  
788 RECEPTOR-LIKE genes mediate leaf-to-leaf wound signalling. *Nature* **500**: 422-426

789 **Murashige T, Skoog F** (1962) A revised medium for rapid growth and bioassays with tobacco tissue  
790 cultures. *Physiol Plant* **15**: 473-497

791 **Navazio L, Bewell MA, Siddiqua A, Dickinson GD, Galione A, Sanders D** (2000) Calcium release

792 from the endoplasmic reticulum of higher plants elicited by the NADP metabolite nicotinic acid adenine  
793 dinucleotide phosphate. Proc Natl Acad Sci USA **97**: 8693-8698

794 **Nagai T, Yamada S, Tominaga T, Ichikawa M, Miyawaki A** (2004) Expanded dynamic range of  
795 fluorescent indicators for Ca<sup>2+</sup> by circularly permuted yellow fluorescent proteins. Proc Natl Acad Sci  
796 USA **101**: 10554-10559

797 **Nakai J, Ohkura M, Imoto K** (2001) A high signal-to-noise Ca<sup>2+</sup> probe composed of a single green  
798 fluorescent protein. Nat Biotechnol **19**: 137-141

799 **Nelson BK, Cai X, Nebenführ A** (2007) A multicolored set of *in vivo* organelle markers for co-  
800 localization studies in Arabidopsis and other plants. Plant J **51**: 1126–1136

801 **Nguyen CT, Kurenda A, Stolz S, Chételat A, Farmer EE** (2018) Identification of cell populations  
802 necessary for leaf-to-leaf electrical signaling in a wounded plant. Proc Natl Acad Sci USA **115**: 10178-  
803 10183

804 **Palmer AE, Giacomello M, Kortemme T, Hires SA, Lev-Ram V, Baker D, Tsien RY** (2006) Ca<sup>2+</sup>  
805 indicators based on computationally redesigned calmodulin-peptide pairs. Chem Biol **13**: 521-530

806 **Peragine A, Yoshikawa M, Wu G, Albrecht HL, Poethig RS** (2004) SGS3 and SGS2/SDE1/RDR6  
807 are required for juvenile development and the production of trans-acting siRNAs in Arabidopsis.  
808 Genes Dev **18**: 2368-2379

809 **Resentini F, Ruberti C, Grenzi M, Bonza MC, Costa A** (2021) The signatures of organellar calcium.  
810 Plant Phys. doi. 10.1093/plphys/kiab189

811 **Rodriguez-Enriquez M, Mehdi S, Dickinson H, Grant-Downtown R** (2012) A novel method for  
812 efficient *in vitro* germination and tube growth of Arabidopsis thaliana pollen. New Phytol **197**: 668–679

813 **Schoenaers S, Balcerowicz D, Costa A, Vissenberg K** (2017) The kinase ERULUS controls pollen  
814 tube targeting and growth in *Arabidopsis thaliana*. Front Plant Sci **14**:8: 1942

815 **Shkolnik D, Nuriel R, Bonza MC, Costa A, Fromm H** (2018) MIZ1 regulates ECA1 to generate a

816 slow, long-distance phloem-transmitted  $\text{Ca}^{2+}$  signal essential for root water tracking in Arabidopsis.  
817 Proc Natl Acad Sci USA **115**: 8031-8036

818 **Soboloff J, Rothberg BS, Madesh M, Gill DL** (2012) STIM proteins: dynamic calcium signal  
819 transducers. Nat Rev Mol Cell Biol **13**: 549-565

820 **Tanaka K, Swanson SJ, Gilroy S, Stacey G** (2010) Extracellular nucleotides elicit cytosolic free  
821 calcium oscillations in Arabidopsis. Plant Physiol **154**: 705-719

822 **Tian D, Wang J, Zeng X, Gu K, Qiu C, Yang X, Zhou Z, Goh M, Luo Y, Murata-Hori M, White FF,**  
823 **Yin Z** (2014) The rice TAL effector-dependent resistance protein XA10 triggers cell death and calcium  
824 depletion in the endoplasmic reticulum. Plant Cell **26**: 497-515

825 **Toyota M, Spencer D, Sawai-Toyota S, Jiaqi W, Zhang T, Koo AJ, Howe GA, Gilroy S** (2018)  
826 Glutamate triggers long-distance, calcium-based plant defense signaling. Science **361**: 1112-1115

827 **Vigani G, Costa A** (2019) Harnessing the new emerging imaging technologies to uncover the role of  
828  $\text{Ca}^{2+}$  signalling in plant nutrient homeostasis. Plant Cell Environ **42**: 2885-2901

829 **Vincent TR, Avramova M, Canham J, Higgins P, Bilkey N, Mugford ST, Pitino M, Toyota M,**  
830 **Gilroy S, Miller AJ, Hogenhout SA, Sanders D** (2017) Interplay of plasma membrane and vacuolar  
831 ion channels, together with BAK1, elicits rapid cytosolic calcium elevations in Arabidopsis during aphid  
832 feeding. Plant Cell **29**: 1460-1479

833 **Waadt R, Krebs M, Kudla J, Schumacher K** (2017) Multiparameter imaging of calcium and abscisic  
834 acid and high-resolution quantitative calcium measurements using R-GECO1-mTurquoise in  
835 Arabidopsis. New Phytol **216**: 303-320

836 **Waadt R, Kudla J** (2008) In planta visualization of protein interactions using bimolecular fluorescence  
837 complementation (BiFC). Cold Spring Harb Protoc 2008: pdb.prot4995

838 **Zhao Y, Araki S, Wu J, Teramoto T, Chang YF, Nakano M, Abdelfattah AS, Fujiwara M, Ishihara**  
839 **T, Nagai T, Campbell RE** (2011) An expanded palette of genetically encoded  $\text{Ca}^{2+}$  indicators.



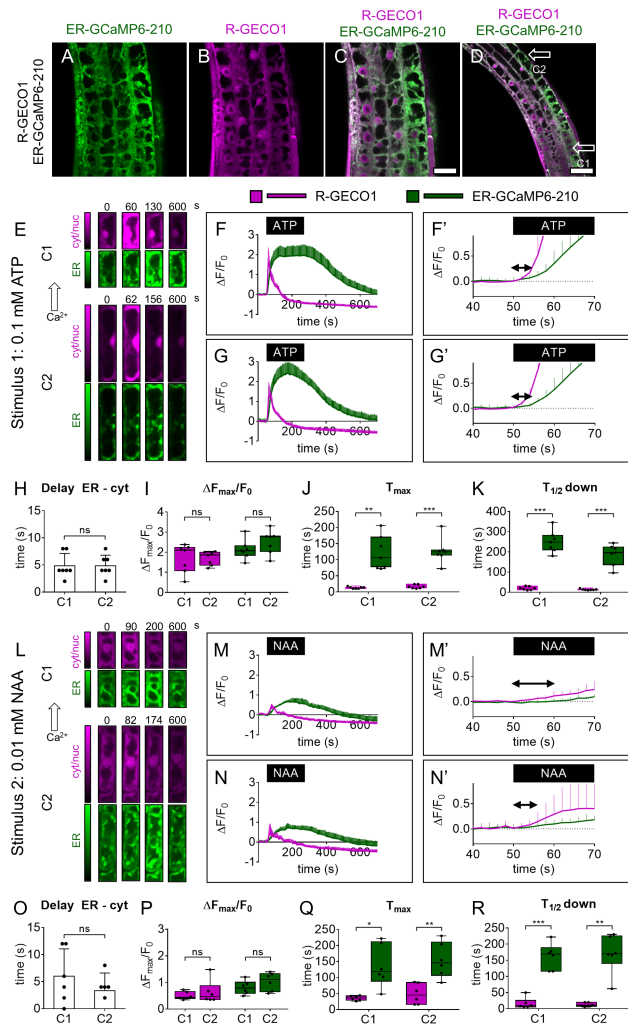


**Figure 1.** Simultaneous cytosolic and ER  $\text{Ca}^{2+}$  analyses in root tip at the single-cell level. (A–D) Images of root-tip cells of a representative pUBQ10-ER-GCaMP6-210 x pUBQ10-R-GECO1 seedling. (A) Green: ER-GCaMP6-210 fluorescence. (B) Magenta: R-GECO1 fluorescence. (C) Overlay of (A) and (B). Scale bar 25  $\mu\text{m}$ . (D) Lower magnification image of (C). Scale bar 50  $\mu\text{m}$ . (E) Exemplary false-color images illustrate R-GECO1 (magenta) and ER-GCaMP6-210 (green) of cell 1 (C1) and cell 2 (C2) in root tips of seedlings expressing simultaneously the two  $\text{Ca}^{2+}$  sensors at steady-state and during the  $\text{Ca}^{2+}$  transient induced by the treatment with 0.1 mM ATP for 3 min. (F) R-GECO1 and ER-GCaMP6-210 normalized fluorescence changes of C1 over the time acquired under continuous perfusion and treated with 0.1 mM ATP for 3 min, as indicated by the black box on the x-axis. (F') same as panel (F) but x-axis, y-axis scales, and ranges adjusted. (G) R-GECO1 and ER-GCaMP6-210 normalized fluorescence changes of C2 over the time acquired under continuous perfusion and treated with 0.1 mM ATP for 3 min, as indicated by the black box on the x-axis. (G') same as panel (G) but x-axis, y-axis scales, and ranges adjusted. The double arrow in (F') and (G') indicates the delay time quantified in (H). (H) Mean delay of the fluorescence increase of the ER-GCaMP6-210 compared to the fluorescence change of the R-GECO1 for C1 and C2 following 0.1 mM ATP administration. (I) Maximal peaks of ER-GCaMP6-210 and R-GECO1 fluorescence signals for C1 and C2 after 0.1 mM ATP administration. (J) Time required to reach maximal peaks of ER-GCaMP6-210 and R-GECO1 fluorescence emissions for C1 and C2 after stimulus administration. (K) Time required to pass half-maximal ER-GCaMP6-210 and R-GECO1 fluorescence signals during recovery after the stimulus.  $n = 7$ . (L) Exemplary false-color images illustrate R-GECO1 (magenta) and ER-GCaMP6-210 (green) of C1 and C2 in root tips of seedlings expressing simultaneously the two  $\text{Ca}^{2+}$  sensors, at steady-state and during the  $\text{Ca}^{2+}$  increase induced by the treatment with 0.01 mM NAA for 3 min. (M) R-GECO1 and ER-GCaMP6-210 normalized fluorescence changes of C1 over the time acquired under continuous perfusion and treated with 0.01 mM NAA for 3 min, as indicated by the black box on the x-axis. (M') same as panel (M) but x-axis, y-axis scales, and ranges adjusted. (N) R-GECO1 and ER-GCaMP6-210 normalized fluorescence changes of C2 over the time acquired under continuous perfusion and treated with 0.01 mM NAA for 3 min, as indicated by the black box on the x-axis. (N') same as panel (N) but x-axis, y-axis scales, and ranges adjusted. The double arrow in (M') and (N') indicates the delay time quantified in (O). (O) Mean delay of the fluorescence increase of the ER-GCaMP6-210 compared to the fluorescence change of the R-GECO1 for C1 and C2 following 0.01 mM NAA administration. (P) Maximal peaks of ER-GCaMP6-210 and R-GECO1 fluorescence signals for C1 and C2 after 0.01 mM NAA administration. (Q) Time required to reach maximal peaks of ER-GCaMP6-210 and R-GECO1 fluorescence signals for C1 and C2 after stimulus administration. (R) Time required to pass half-maximal ER-GCaMP6-210 and R-GECO1 fluorescence emissions during recovery after the stimulus.  $n = 6$ . Error bars = SD, ns = not significant, \* $p \leq 0.05$ , \*\* $p \leq 0.005$ , \*\*\* $p \leq 0.0005$  (Student's *t*-test).

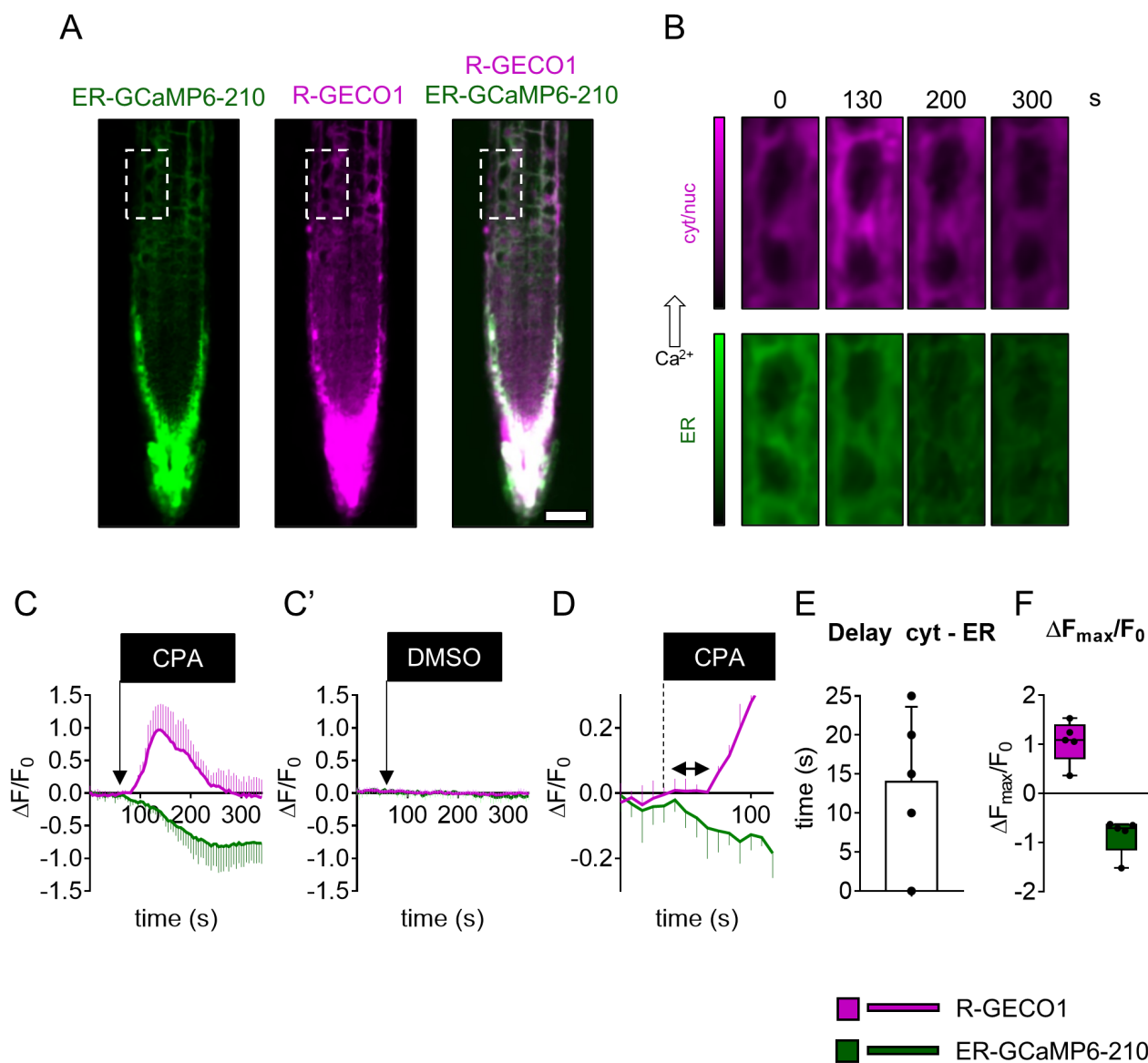


**Figure 2.** Simultaneous cytosolic and ER Ca<sup>2+</sup> analyses in root-tip cells treated with the P-Type IIA inhibitor cyclopiazonic acid (CPA). **(A)** Green: ER-GCaMP6-210 fluorescence, Magenta: R-GECO1 fluorescence, and overlay. Scale bar 50  $\mu$ m. **(B)** Examples of false-color images illustrate R-GECO1 (magenta) and ER-GCaMP6-210 (green) of the selected cell (dashed rectangle in (A)) in root tips of seedlings expressing simultaneously the two Ca<sup>2+</sup> sensors at steady-state and during the Ca<sup>2+</sup> treatment with 25  $\mu$ M CPA for 3 min. **(C)** R-GECO1 and ER-GCaMP6-210 normalized fluorescence changes of the selected cell over the time acquired under continuous perfusion and treated with 25  $\mu$ M CPA for 3 min, as indicated by the black box on the x-axis. **(C')** R-GECO1 and ER-GCaMP6-210 normalized fluorescence of the selected cell over the time acquired under continuous perfusion and treated with DMSO (the CPA solvent) as a control for 3 min, as indicated by the black box on the x-axis. **(D)** same as panel (C) but x-axis, y-axis scales, and ranges adjusted. The double arrow in (D) indicates the delay time quantified in (E). **(E)** Mean delay of the fluorescence increase of the R-GECO1 following the ER-GCaMP6-210 fluorescence decrease. **(F)** The maximal peak of R-GECO1 and the minimal level of ER-GCaMP6-210 fluorescence signals for the selected cells after CPA administration. n = 5. Error bars = SD.



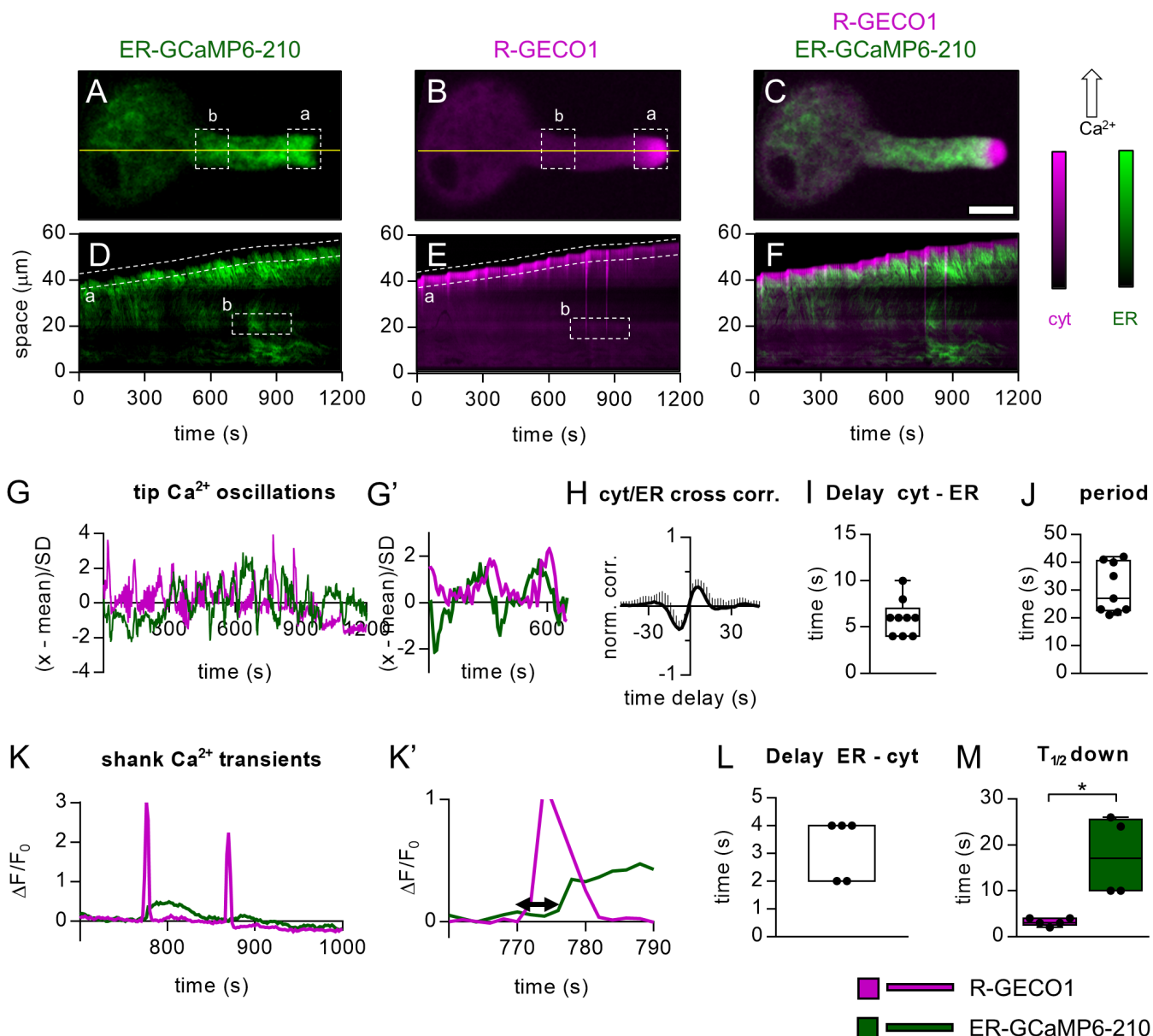


**Figure 3.** Simultaneous ER-GCaMP6-210 and R-GECO1 fluorescence signals in growing pollen tubes. **(A-C)** Images of a representative pollen tube. **(A)** Green: ER-GCaMP6-210 fluorescence. **(B)** Magenta: R-GECO1 fluorescence. **(C)** Overlay of (A) and (B). Scale bar 20  $\mu\text{m}$ . **(D-F)** Kymograph extracted from both fluorescence signals frames by observing the temporal evolution of the pixel line highlighted in yellow. **(D)** Kymograph of 1200 s acquisitions extracted for the R-GECO1 images. **(E)** Kymograph of 1200 s acquisitions extracted for the ER-GCaMP6-210 images. **(F)** Overlay of (D) and (E). (a) = selected ROI for analyses of pollen tube tip fluorescence signals. (b) selected ROI for analyses of pollen tube shank fluorescence signals. **(G)** Representative oscillations of ER-GCaMP6-210 and R-GECO1 fluorescences in the tip (ROI "a"). **(G')** same as panel (G) but x-axis, y-axis scales, and ranges adjusted. **(H)** Normalized cross-correlation analysis between R-GECO1 and ER-GCaMP6-210 averaged in temporal sliding windows of 80 s over n = 9 measurements. The peak-value is  $0.28 \pm 0.11$ , and it is reached at positive delays, implying that the fast oscillations in the cytosol (R-GECO1) are anticipated by the ones in the ER (ER-GCaMP6-210). **(I)** Distribution of the average delays by locating in time the maximum of the cross-correlations, for each experiment considered. The global temporal lag is  $6 \pm 2$  s. **(J)** Distribution of the period of the fast oscillations in the ER/Cytosol. It is defined by doubling the temporal distance at which the signals correlate (maximum in G) and anticorrelates (minimum). The average is  $30 \pm 11$  s. **(K)** Representative ER-GCaMP6-210 and R-GECO1 fluorescences in the shank (ROI "b"). **(K')** same as panel (K) but x-axis, y-axis scales and ranges adjusted. The double arrow in (K') indicates the delay time quantified in (L). **(L)** Mean delay of the fluorescence increase of the ER-GCaMP6-210 compared to the fluorescence change of the R-GECO1. **(M)** Time required to pass half-maximal ER-GCaMP6-210 and R-GECO1 fluorescence emissions during recovery after the spike. n = 5. Error bars = SD, \*p  $\leq 0.05$  (Student's t-test).



## Parsed Citations

Aller I, Rouhier N, Meyer AJ (2013) Development of roGFP2-derived redox probes for measurement of the glutathione redox potential in the cytosol of severely glutathione-deficient *rml1* seedlings. *Front Plant Sci* 16:4:506.

Google Scholar: [Author Only](#) [Title Only](#) [Author and Title](#)

Amack SC, Antunes MS (2020) CaMV35S promoter – A plant biology and biotechnology workhorse in the era of synthetic biology. *Curr Plant Biol* 24: 100179

Google Scholar: [Author Only](#) [Title Only](#) [Author and Title](#)

Baird GS, Zacharias DA, Tsien RY (1999) Circular permutation and receptor insertion within green fluorescent proteins. *Proc Natl Acad Sci USA* 96: 11241-11246

Google Scholar: [Author Only](#) [Title Only](#) [Author and Title](#)

Barberini ML, Sigaut L, Huang W, Mangano S, Juarez SPD, Marzol E, Estevez J, Obertello M, Pietrasanta L, Tang W, Muschietti J (2018) Calcium dynamics in tomato pollen tubes using the Yellow Cameleon 3.6 sensor. *Plant Reprod* 31:159-169

Google Scholar: [Author Only](#) [Title Only](#) [Author and Title](#)

Behera S, Kudla J (2013) High-resolution imaging of cytoplasmic Ca<sup>2+</sup> dynamics in *Arabidopsis* roots. *Cold Spring Harb Protoc* 2013: 665-669

Google Scholar: [Author Only](#) [Title Only](#) [Author and Title](#)

Behera S, Xu Z, Luoni L, Bonza MC, Doccu FG, De Michelis MI, Morris RJ, Schwarzländer M, Costa A (2018) Cellular Ca<sup>2+</sup> Signals Generate Defined pH Signatures in Plants. *Plant Cell* 30: 2704-2719

Google Scholar: [Author Only](#) [Title Only](#) [Author and Title](#)

Bonza, M.C., De Michelis, M.I. (2011). The plant Ca<sup>2+</sup>-ATPase repertoire: biochemical features and physiological functions. *Plant Biol*. 13: 421-430

Google Scholar: [Author Only](#) [Title Only](#) [Author and Title](#)

Bonza, M.C., Loro, G., Behera, S., Wong, A, Kudla, J., Costa, A. (2013). Analyses of Ca<sup>2+</sup> accumulation and dynamics in the endoplasmic reticulum of *Arabidopsis* root cells using a genetically encoded Cameleon sensor. *Plant Physiol*. 163: 1230-1241

Google Scholar: [Author Only](#) [Title Only](#) [Author and Title](#)

Brandizzi F, Fricker M, Hawes C (2002) A greener world: the revolution in plant bioimaging. *Nat Rev Mol Cell Biol* 3: 520-530

Google Scholar: [Author Only](#) [Title Only](#) [Author and Title](#)

Charpentier M, Sun J, Vaz Martins T, Radhakrishnan GV, Findlay K, Soumpourou E, Thouin J, Very AA, Sanders D, Morris RJ, Oldroyd GE (2016) Nuclear-localized cyclic nucleotide-gated channels mediate symbiotic calcium oscillations. *Science* 352: 1102-1105

Google Scholar: [Author Only](#) [Title Only](#) [Author and Title](#)

Chen TW, Wardill TJ, Sun Y, Pulver SR, Renninger SL, Baohan A, Schreiter ER, Kerr RA, Orger MB, Jayaraman V, Looger LL, Svoboda K, Kim DS (2013) Ultrasensitive fluorescent proteins for imaging neuronal activity. *Nature* 499: 295-300

Google Scholar: [Author Only](#) [Title Only](#) [Author and Title](#)

Clough SJ, Bent AF (1998) Floral dip: a simplified method for *Agrobacterium*-mediated transformation of *Arabidopsis thaliana*. *Plant J* 16: 735-743

Google Scholar: [Author Only](#) [Title Only](#) [Author and Title](#)

Corso M, Doccu FG, de Melo JRF, Costa A, Verbruggen N (2018) Endoplasmic reticulum-localized CCX2 is required for osmotolerance by regulating ER and cytosolic Ca<sup>2+</sup> dynamics in *Arabidopsis*. *Proc Natl Acad Sci USA* 115: 3966-3971

Google Scholar: [Author Only](#) [Title Only](#) [Author and Title](#)

Costa A, Candeo A, Fieramonti L, Valentini G, Bassi A (2013) Calcium dynamics in root cells of *Arabidopsis thaliana* visualized with selective plane illumination microscopy. *PLoS One* 16;8(10):e75646.

Google Scholar: [Author Only](#) [Title Only](#) [Author and Title](#)

Damineli DSC, Portes MT, Feijó JA (2017) Oscillatory signatures underlie growth regimes in *Arabidopsis* pollen tubes: computational methods to estimate tip location, periodicity, and synchronization in growing cells. *J Exp Bot* 68: 3267-3281

Google Scholar: [Author Only](#) [Title Only](#) [Author and Title](#)

De Col V, Fuchs P, Nietzel T, Elsässer M, Voon CP, Candeo A, Seeliger I, Fricker MD, Grefen C, Møller IM, Bassi A, Lim BL, Zancani M, Meyer AJ, Costa A, Wagner S, Schwarzländer M (2017) ATP sensing in living plant cells reveals tissue gradients and stress dynamics of energy physiology. *Elife* 18;6:e26770

Google Scholar: [Author Only](#) [Title Only](#) [Author and Title](#)

de Juan-Sanz J, Holt GT, Schreiter ER, de Juan F, Kim DS, Ryan TA (2017) Axonal endoplasmic reticulum Ca<sup>2+</sup> content controls release probability in CNS nerve terminals. *Neuron* 93: 867-881

Google Scholar: [Author Only](#) [Title Only](#) [Author and Title](#)

Edel KH, Marchadier E, Brownlee C, Kudla J, Hetherington AM (2017) The evolution of calcium-based signalling in plants. *Curr Biol* 27: R667-r679

Google Scholar: [Author Only](#) [Title Only](#) [Author and Title](#)

- Feijó JA, Costa SS, Prado AM, Becker JD, Certal AC (2004) Signalling by tips. *Curr Opin Plant Biol* 7: 589-598  
Google Scholar: [Author Only](#) [Title Only](#) [Author and Title](#)
- Foskett JK, White C, Cheung KH, Mak DO (2007) Inositol trisphosphate receptor Ca<sup>2+</sup> release channels. *Physiol Rev* 87: 593-658  
Google Scholar: [Author Only](#) [Title Only](#) [Author and Title](#)
- Franklin-Tong VE, Drobak BK, Allan AC, Watkins P, Trewavas AJ (1996) Growth of pollen tubes of *Papaver rhoeas* is regulated by a slow-moving calcium wave propagated by inositol 1,4,5-trisphosphate. *Plant Cell* 8: 1305-1321  
Google Scholar: [Author Only](#) [Title Only](#) [Author and Title](#)
- Grefen C, Donald N, Hashimoto K, Kudla J, Schumacher K, Blatt MR (2010) A ubiquitin-10 promoter-based vector set for fluorescent protein tagging facilitates temporal stability and native protein distribution in transient and stable expression studies. *Plant J* 64: 355-365  
Google Scholar: [Author Only](#) [Title Only](#) [Author and Title](#)
- Greotti E, Wong A, Pozzan T, Penden D, Pizzo P (2016) Characterization of the ER-Targeted Low Affinity Ca<sup>2+</sup> Probe D4ER. *Sensors (Basel)*. 16(9):1419  
Google Scholar: [Author Only](#) [Title Only](#) [Author and Title](#)
- Hellens RP, Edwards EA, Leyland NR, Bean S, Mullineaux PM (2000) pGreen: a versatile and flexible binary Ti vector for *Agrobacterium*-mediated plant transformation. *Plant Mol Biol* 42: 819-832  
Google Scholar: [Author Only](#) [Title Only](#) [Author and Title](#)
- Holdaway-Clarke TL, Feijo JA, Hackett GR, Kunkel JG, Hepler PK (1997) Pollen tube growth and the intracellular cytosolic calcium gradient oscillate in phase while extracellular calcium influx is delayed. *Plant Cell* 9: 1999-2010  
Google Scholar: [Author Only](#) [Title Only](#) [Author and Title](#)
- Iwano M, Entani T, Shiba H, Kakita M, Nagai T, Mizuno H, Miyawaki A, Shoji T, Kubo K, Isogai A, Takayama S (2009) Fine-tuning of the cytoplasmic Ca<sup>2+</sup> concentration is essential for pollen tube growth. *Plant Physiol* 150: 1322-1334  
Google Scholar: [Author Only](#) [Title Only](#) [Author and Title](#)
- Ishka MR, Brown E, Rosenberg A, Romanowsky S, Davis J, Choi W-G, Harper JF (2021) Arabidopsis Ca<sup>2+</sup>-ATPases 1, 2, and 7 in the endoplasmic reticulum contribute to growth and pollen fitness. *Plant Physiol* doi.org/10.1093/plphys/kiab021  
Google Scholar: [Author Only](#) [Title Only](#) [Author and Title](#)
- Johns S, Hagihara T, Toyota M, Gilroy S (2021) The Fast and The Furious: Rapid long-range signaling in plants. *Plant Physiol* doi.org/10.1093/plphys/kiab098  
Google Scholar: [Author Only](#) [Title Only](#) [Author and Title](#)
- Keinath NF, Waadt R, Brugman R, Schroeder JI, Grossmann G, Schumacher K, Krebs M (2015) Live cell imaging with R-GECO1 sheds light on flg22- and chitin-induced transient [Ca<sup>2+</sup>]<sub>cyt</sub> patterns in Arabidopsis. *Mol Plant* 8: 1188-1200  
Google Scholar: [Author Only](#) [Title Only](#) [Author and Title](#)
- Leitão N, Dangeville P, Carter R, Charpentier M (2019) Nuclear calcium signatures are associated with root development. *Nat Commun* 25:10(1):4865  
Google Scholar: [Author Only](#) [Title Only](#) [Author and Title](#)
- Li K, Prada J, Daminieli DSC, Liese A, Romeis T, Dandekar T, Feijó JA, Hedrich R, Konrad KR (2021) An optimized genetically encoded dual reporter for simultaneous ratio imaging of Ca<sup>2+</sup> and H<sup>+</sup> reveals new insights into ion signaling in plants. *New Phytol* doi: 10.1111/nph.17202.  
Google Scholar: [Author Only](#) [Title Only](#) [Author and Title](#)
- Liang F, Sze H (1998) A high-affinity Ca<sup>2+</sup> pump, ECA1, from the endoplasmic reticulum is inhibited by cyclopiazonic acid but not by thapsigargin. *Plant Physiol* 118: 817-825  
Google Scholar: [Author Only](#) [Title Only](#) [Author and Title](#)
- Lovy-Wheeler A, Cárdenas L, Kunkel JG, Hepler PK (2007) Differential organelle movement on the actin cytoskeleton in lily pollen tubes. *Cell Motil Cytoskeleton* 64: 217-232  
Google Scholar: [Author Only](#) [Title Only](#) [Author and Title](#)
- Luo J, Chen L, Huang F, Gao P, Zhao H, Wang Y, Han S (2020) Intraorganellar calcium imaging in Arabidopsis seedling roots using the GCaMP variants GCaMP6m and R-CEPIA1er. *J Plant Physiol* 246-247:153127  
Google Scholar: [Author Only](#) [Title Only](#) [Author and Title](#)
- Martinière A, Bassil E, Jublanc E, Alcon C, Reguera M, Sentenac H, Blumwald E, Paris N (2013) In vivo intracellular pH measurements in tobacco and Arabidopsis reveal an unexpected pH gradient in the endomembrane system. *Plant Cell* 25: 4028-4043  
Google Scholar: [Author Only](#) [Title Only](#) [Author and Title](#)
- Mousavi SA, Chauvin A, Pascaud F, Kellenberger S, Farmer EE (2013) GLUTAMATE RECEPTOR-LIKE genes mediate leaf-to-leaf wound signalling. *Nature* 500: 422-426  
Google Scholar: [Author Only](#) [Title Only](#) [Author and Title](#)
- Murashige T, Skoog F (1962) A revised medium for rapid growth and bioassays with tobacco tissue cultures. *Physiol Plant* 15: 473-497

Google Scholar: [Author Only](#) [Title Only](#) [Author and Title](#)

Navazio L, Bewell MA, Siddiqua A, Dickinson GD, Galione A, Sanders D (2000) Calcium release from the endoplasmic reticulum of higher plants elicited by the NADP metabolite nicotinic acid adenine dinucleotide phosphate. *Proc Natl Acad Sci USA* 97: 8693-8698

Google Scholar: [Author Only](#) [Title Only](#) [Author and Title](#)

Nagai T, Yamada S, Tominaga T, Ichikawa M, Miyawaki A (2004) Expanded dynamic range of fluorescent indicators for Ca<sup>2+</sup> by circularly permuted yellow fluorescent proteins. *Proc Natl Acad Sci USA* 101: 10554-10559

Google Scholar: [Author Only](#) [Title Only](#) [Author and Title](#)

Nakai J, Ohkura M, Imoto K (2001) A high signal-to-noise Ca<sup>2+</sup> probe composed of a single green fluorescent protein. *Nat Biotechnol* 19: 137-141

Google Scholar: [Author Only](#) [Title Only](#) [Author and Title](#)

Nelson BK, Cai X, Nebenführ A (2007) A multicolored set of in vivo organelle markers for co-localization studies in *Arabidopsis* and other plants. *Plant J* 51: 1126-1136

Google Scholar: [Author Only](#) [Title Only](#) [Author and Title](#)

Nguyen CT, Kurenda A, Stolz S, Chételat A, Farmer EE (2018) Identification of cell populations necessary for leaf-to-leaf electrical signaling in a wounded plant. *Proc Natl Acad Sci USA* 115: 10178-10183

Google Scholar: [Author Only](#) [Title Only](#) [Author and Title](#)

Palmer AE, Giacomello M, Kortemme T, Hires SA, Lev-Ram V, Baker D, Tsien RY (2006) Ca<sup>2+</sup> indicators based on computationally redesigned calmodulin-peptide pairs. *Chem Biol* 13: 521-530

Google Scholar: [Author Only](#) [Title Only](#) [Author and Title](#)

Peragine A, Yoshikawa M, Wu G, Albrecht HL, Poethig RS (2004) SGS3 and SGS2/SDE1/RDR6 are required for juvenile development and the production of trans-acting siRNAs in *Arabidopsis*. *Genes Dev* 18: 2368-2379

Google Scholar: [Author Only](#) [Title Only](#) [Author and Title](#)

Resentini F, Ruberti C, Grenzi M, Bonza MC, Costa A (2021) The signatures of organellar calcium. *Plant Phys*. doi. 10.1093/plphys/kiab189

Google Scholar: [Author Only](#) [Title Only](#) [Author and Title](#)

Rodriguez-Enriquez M, Mehdi S, Dickinson H, Grant-Downtown R (2012) A novel method for efficient in vitro germination and tube growth of *Arabidopsis thaliana* pollen. *New Phytol* 197: 668-679

Google Scholar: [Author Only](#) [Title Only](#) [Author and Title](#)

Schoenaers S, Balcerowicz D, Costa A, Vissenberg K (2017) The kinase ERULUS controls pollen tube targeting and growth in *Arabidopsis thaliana*. *Front Plant Sci* 14:8: 1942

Google Scholar: [Author Only](#) [Title Only](#) [Author and Title](#)

Shkolnik D, Nuriel R, Bonza MC, Costa A, Fromm H (2018) MIZ1 regulates ECA1 to generate a slow, long-distance phloem-transmitted Ca<sup>2+</sup> signal essential for root water tracking in *Arabidopsis*. *Proc Natl Acad Sci USA* 115: 8031-8036

Google Scholar: [Author Only](#) [Title Only](#) [Author and Title](#)

Soboloff J, Rothberg BS, Madesh M, Gill DL (2012) STIM proteins: dynamic calcium signal transducers. *Nat Rev Mol Cell Biol* 13: 549-565

Google Scholar: [Author Only](#) [Title Only](#) [Author and Title](#)

Tanaka K, Swanson SJ, Gilroy S, Stacey G (2010) Extracellular nucleotides elicit cytosolic free calcium oscillations in *Arabidopsis*. *Plant Physiol* 154: 705-719

Google Scholar: [Author Only](#) [Title Only](#) [Author and Title](#)

Tian D, Wang J, Zeng X, Gu K, Qiu C, Yang X, Zhou Z, Goh M, Luo Y, Murata-Hori M, White FF, Yin Z (2014) The rice TAL effector-dependent resistance protein XA10 triggers cell death and calcium depletion in the endoplasmic reticulum. *Plant Cell* 26: 497-515

Google Scholar: [Author Only](#) [Title Only](#) [Author and Title](#)

Toyota M, Spencer D, Sawai-Toyota S, Jiaqi W, Zhang T, Koo AJ, Howe GA, Gilroy S (2018) Glutamate triggers long-distance, calcium-based plant defense signaling. *Science* 361: 1112-1115

Google Scholar: [Author Only](#) [Title Only](#) [Author and Title](#)

Vigani G, Costa A (2019) Harnessing the new emerging imaging technologies to uncover the role of Ca<sup>2+</sup> signalling in plant nutrient homeostasis. *Plant Cell Environ* 42: 2885-2901

Google Scholar: [Author Only](#) [Title Only](#) [Author and Title](#)

Vincent TR, Avramova M, Canham J, Higgins P, Bilkey N, Mugford ST, Pitino M, Toyota M, Gilroy S, Miller AJ, Hogenhout SA, Sanders D (2017) Interplay of plasma membrane and vacuolar ion channels, together with BAK1, elicits rapid cytosolic calcium elevations in *Arabidopsis* during aphid feeding. *Plant Cell* 29: 1460-1479

Google Scholar: [Author Only](#) [Title Only](#) [Author and Title](#)

Waadt R, Krebs M, Kudla J, Schumacher K (2017) Multiparameter imaging of calcium and abscisic acid and high-resolution quantitative calcium measurements using R-GECO1-mTurquoise in *Arabidopsis*. *New Phytol* 216: 303-320

Google Scholar: [Author Only](#) [Title Only](#) [Author and Title](#)

Waadts R, Kudla J (2008) In planta visualization of protein interactions using bimolecular fluorescence complementation (BiFC). Cold Spring Harb Protoc 2008: pdb.prot4995

Google Scholar: [Author Only](#) [Title Only](#) [Author and Title](#)

Zhao Y, Araki S, Wu J, Teramoto T, Chang YF, Nakano M, Abdelfattah AS, Fujiwara M, Ishihara T, Nagai T, Campbell RE (2011) An expanded palette of genetically encoded Ca<sup>2+</sup> indicators. Science 333: 1888-1891

Google Scholar: [Author Only](#) [Title Only](#) [Author and Title](#)